

CONFIDENTIAL

UNCLASSIFIED

Copy 6
RM L50G14

NACA RM L50G14

OCT 10 1950

~~11/16~~
0.2



RESEARCH MEMORANDUM

AERODYNAMIC CHARACTERISTICS AT A MACH NUMBER OF 1.38
OF FOUR WINGS OF ASPECT RATIO 4 HAVING QUARTER-
CHORD SWEEP ANGLES OF 0°, 35°, 45°, AND 60°

By William B. Kemp, Jr., Kenneth W. Goodson,
and Robert A. Booth

Langley Aeronautical Laboratory
Langley Air Force Base, Va.

CLASSIFICATION CANCELLED

Authority *NACA R 72549* Date *8/23/54*

By *NACA 9/8/54* See

CLASSIFIED DOCUMENT

This document contains classified information affecting the National Defense of the United States within the meaning of the Espionage Act, USC 5031 and 32. Its transmission or the revelation of its contents in any manner to an unauthorized person is prohibited by law.

Information so classified may be imparted only to persons in the military and naval services of the United States, appropriate civilian officers and employees of the Federal Government who have a legitimate interest therein, and to United States citizens of known loyalty and discretion who of necessity must be informed thereof.

NATIONAL ADVISORY COMMITTEE FOR AERONAUTICS

WASHINGTON

October 10, 1950

CONFIDENTIAL

UNCLASSIFIED



UNCLASSIFIED

NATIONAL ADVISORY COMMITTEE FOR AERONAUTICS

RESEARCH MEMORANDUM

AERODYNAMIC CHARACTERISTICS AT A MACH NUMBER OF 1.38

OF FOUR WINGS OF ASPECT RATIO 4 HAVING QUARTER-
CHORD SWEEP ANGLES OF 0° , 35° , 45° , AND 60°

By William B. Kemp, Jr., Kenneth W. Goodson,
and Robert A. Booth

SUMMARY

A description of the Langley 6-inch supersonic tunnel is presented together with results of tests conducted at a Mach number of 1.38 and a Reynolds number of 390,000, to determine the supersonic aerodynamic characteristics of four sweptback wings and wing-body configurations. The wings were all of aspect ratio 4, taper ratio 0.6, and NACA 65A006 airfoil section. The sweepback angles used were 0° , 35° , 45° , and 60° .

At the low Reynolds number of the present tests, laminar separation occurred near the trailing edge of all wings producing reduced stability in the low-lift range. The effects of increasing angle of sweepback were to reduce the lift-curve slope and zero-lift drag coefficient, to increase the maximum lift-drag ratio, and to produce an outward shift in the lateral center of pressure. The measured lift-curve slopes were less for all wings than those predicted from linearized theory. Good agreement was obtained between theoretical and experimental aerodynamic-center location in the lift-coefficient range not affected by separation effects for sweep angles up to 45° . For the 60° sweptback wing at lift coefficients above 0.25, a leading-edge separation vortex produced severe instability with reduced lift and increased drag. At lift coefficients below 0.25, this wing exhibited a considerable proportion of the theoretically available leading-edge suction. Addition of either leading-edge roughness, blunt trailing edge, or a fence to the 60° wing improved the stability characteristics at low lift coefficients. The fence also decreased the instability of the 60° wing at high lift coefficients.

UNCLASSIFIED

INTRODUCTION

An investigation has been made in the Langley 6-inch supersonic tunnel to determine the general stability characteristics of a series of sweptback wings and wing-body combinations. Each wing had an aspect ratio of 4, a taper ratio of 0.6, and NACA 65A006 airfoil sections. Semispan wings having sweepback angles of 0° , 35° , 45° , and 60° of the quarter-chord line were investigated. Data were obtained at a Mach number of 1.38, thus extending the speed range of the data obtained by the transonic-bump technique (references 1, 2, 3, and 4) on wings of identical plan form and airfoil section.

The results of the investigation at a Mach number of 1.38 and a Reynolds number of 390,000 together with a description of the Langley 6-inch supersonic tunnel are given in the present paper.

COEFFICIENTS AND SYMBOLS

C_L	lift coefficient	$\left(\frac{\text{Measured lift}}{qS/2} \right)$
C_D	drag coefficient	$\left(\frac{\text{Measured drag}}{qS/2} \right)$
ΔC_D	drag coefficient due to lift	
C_{D_0}	drag coefficient at zero lift	
C_m	pitching-moment coefficient referred to $0.25\bar{c}$	$\left(\frac{\text{Measured pitching moment}}{q \frac{S}{2} \bar{c}} \right)$
C_B	bending-moment coefficient about root chord	$\left(\frac{\text{Measured bending moment}}{q \frac{S}{2} \frac{b}{2}} \right)$
q	dynamic pressure, pounds per square foot	$\left(\frac{1}{2} \rho V^2 \right)$

S	twice wing area of semispan model, 0.045 square foot
\bar{c}	mean aerodynamic chord of wing, 0.108 foot $\left(\frac{2}{S} \int_0^{b/2} c^2 dy \right)$
c	local wing chord, feet
b	twice span of semispan model, feet
y	lateral distance from plane of symmetry, feet
X	distance downstream of test section center line, inches
Y	lateral distance from left tunnel wall, inches
ρ	air density, slugs per cubic foot
V	airspeed, feet per second
M	Mach number
Λ	sweep angle of quarter-chord line, degrees
α	angle of attack of root chord, degrees
y_{cp}	lateral center of pressure, percent semispan $\left(100C_B/C_L \right)$
P_T	local stagnation pressure behind a normal shock
P_{T_0}	free-stream stagnation pressure behind a normal shock
L/D	ratio of lift to drag
$C_{L\alpha}$	$= \frac{\partial C_L}{\partial \alpha}$

DESCRIPTION OF APPARATUS

The Langley 6-inch supersonic tunnel in which the tests were conducted is a closed-return, continuous-operation tunnel with a nozzle capable of producing a fixed test Mach number of 1.38 in a 6-inch-square test section. A photograph showing the general arrangement of the tunnel

~~CONFIDENTIAL~~

is given in figure 1. The tunnel is powered by a two-stage counter-rotating axial-flow blower driven by two 110-horsepower water-cooled electric motors. Cooling of the tunnel is accomplished by exchange of atmospheric air. The amount of cooling air induced is controlled so that the stagnation temperature in the test section during operation is normally greater than 180° F. This temperature is high enough to prevent condensation of atmospheric humidity in the test section.

The distribution of Mach number along the test-section center lines, obtained from total- and static-pressure surveys of the clear tunnel is presented in figure 2. Survey results in the tunnel-wall boundary layer are given in figure 3 as the ratio of total-pressure-tube reading in the boundary layer to total-pressure-tube reading in the free stream. At the model mounting position, the wall boundary-layer thickness is of the order of 0.25 inch.

The variation of flow angularity across the test section during the model tests reported in this paper is shown in figure 4 by the curves for the screens-out condition. It is apparent that a large gradient in flow angle existed in the test section, the most severe gradient occurring near the right wall. In order to obtain the least variation of flow angle over the model span, the models were mounted through the left wall and extended only about $2\frac{1}{2}$ inches into the test section. After completion of these model tests, an attempt was made to improve the tunnel airflow by installation of screens. This installation resulted in a practically uniform flow angle in the test section (fig. 4). One of the models was then tested with and without screens to evaluate the effects of the spanwise variation in flow angle which existed during the basic model tests. The results of this evaluation are discussed in another section of this paper. The screens consisted of five panels of 40-mesh bronze wire cloth located in the settling chamber ahead of the nozzle. These screens have now been permanently installed in this tunnel.

A typical model installation is illustrated by the photograph of figure 5. The model is mounted through the left tunnel wall and is attached to a five-component electrical strain-gage balance. The balance is enclosed in a chamber which is sealed except for a gap around the model root. A turntable which rotates as the model angle of attack is changed is installed in the tunnel wall so that the gap around the model root may be held as small as possible (of the order of 0.03 in.). For wing-alone tests the model is shielded from any residual flow through the gap by an end plate 0.021 inch thick spaced 0.025 inch from the wall (shown in fig. 5). For wing-fuselage configurations a half-fuselage replaces the end plate. The relationship between the end plate and the tunnel wall is shown more clearly in the photograph of figure 6. The use of the end plate on the model root has been shown by preliminary

tests to give satisfactory agreement between the partial-span results obtained in the 6-inch supersonic tunnel and full-span results obtained in other facilities. The end plate has been found, however, to produce a small and sensibly constant increment in drag coefficient.

MODELS AND TESTS

Dimensional details of the series of wings and wing-body combinations investigated are given in the two-view drawings of figure 7. Dimensions of the fuselage are given in table I. For each wing-fuselage combination the fuselage was located so that the maximum fuselage diameter was at the same longitudinal position as the quarter-chord point of the wing mean aerodynamic chord. The 0° , 35° , and 60° swept wings were made of solid steel, whereas the 45° swept wing was of solid beryllium copper. In view of the fact that steel has a modulus of elasticity about 1.7 times that of beryllium copper, the difference in the materials of construction would affect the relative deformation of the models under the air loads imposed during the tests.

Several modifications of the 60° sweptback wing were investigated. A thin coat of paint bearing small roughness particles was applied to the wing surface forward of the 10-percent-chord line to promote boundary-layer transition. A blunt trailing edge was formed by building up the rear portion of the airfoil to a trailing-edge thickness equal to one-half the maximum section thickness. Details of the blunt trailing edge are shown in figure 8. An upper-surface fence, shown in figure 9, was attached at the wing mean aerodynamic chord.

The test Reynolds number was about 390,000 for all models based on average values of stagnation temperature and pressure occurring during the tests. The angle-of-attack range of the tests was limited to about 15° . At higher angles, the normal shock of the tunnel moved into the test section and merged with the shock pattern from the model. The pressures on the test-section walls were observed during the tests to ascertain the location of the normal shock, and test data were not obtained after the normal shock moved into the test section.

The test data presented herein were obtained in the tunnel without screens and have been corrected for the average value of the flow angularity over the model span. No correction was applied for the angularity gradients along the span; however, to evaluate the effects of the angularity gradient on the present data, successive tests were made with the 60° -sweptback wing with and without screens. These data are presented in figure 10 and show only minor effects of the screen installation. The effects of the small spanwise gradient of flow angularity may, therefore, be considered negligible.

The estimated probable error in the present data is presented in the following table:

Lift coefficient	±0.0046
Drag coefficient	±0.0012
Pitching-moment coefficient	±0.0027
Bending-moment coefficient	±0.0064
Angle of attack, deg	±0.1

These values were obtained by averaging over the angle-of-attack range the difference between test points of two separate tests of the same model configuration.

RESULTS AND DISCUSSION

Presentation of Results

The results obtained in the tests of the wings investigated are presented in the following figures:

	<u>Figure</u>
Basic wing-alone data..	11
Modifications to 60° wing	12
Basic wing-fuselage data	13
Typical liquid-film photograph	14
Summary of sweep effects	15
Variation of L/D with lift coefficient	16
Drag-rise characteristics	17

Basic Wing Data

Examination of figure 11 indicates that some nonlinearity in the lift and pitching-moment characteristics existed for each wing. The nonlinearities resulted in regions of reduced lift-curve slope barely discernible at low sweep angles, and reduced stability which became more pronounced as the sweep angle increased. In the moderate- and high-lift-coefficient range, results of theoretical calculations based on linearized theory show good agreement with the experimental rate of change of pitching-moment coefficient with lift coefficient for sweep angles up to 45°. At 60° sweep, however, the agreement is poor.

In the low-lift-coefficient range the regions of reduced stability are noticeable in the experimental pitching-moment curves at all sweep

angles. Liquid-film studies have shown that laminar separation occurred on both the upper and lower surfaces of the wings near the trailing edge at 0° angle of attack. An example of a typical liquid-film photograph illustrating this laminar separation is shown in figure 114. A similar occurrence was observed and supported by liquid-film studies in the investigation of reference 5. As the angle of attack was increased above 0° the separated area shifted entirely to the upper surface, producing an effective change in camber with angle of attack which may be considered analogous to the action of a free-floating trailing-edge flap. For the low sweep angles where a supersonic type of pressure distribution exists, a relatively small change in lifting pressure on the wing trailing edge results in a noticeable change in pitching-moment coefficient. For high sweep angles, however, where subsonic type of flow is experienced, adverse pressure gradients are felt over a large part of the wing chord which produce more severe separation effects than those obtained for the lower sweep angles. The change of lifting pressure thus incurred as this separation shifts from one surface to the other affects both the lift and pitching-moment coefficients. This effect became particularly severe at 60° sweep resulting in instability at low angles of attack. (See fig. 11.) As the angle of attack was increased beyond about 2° , liquid-film observations on the 60° swept wing indicated that the laminar separation on the lower surface decreased in extent and, in addition, transition from laminar to turbulent boundary layer occurred on the inboard portion of the upper surface. Thus, in the intermediate-lift-coefficient range, the effects of laminar separation near the trailing edge were considerably less pronounced than at low lift coefficients, resulting in the increased stability and lift-curve slope observed at lift coefficients above 0.1.

At high lift coefficients, the lift-curve slopes and stability parameters were relatively unchanged for the low sweep angles. For high sweep angles, however, a reduction in lift and pitching-moment-curve slopes was observed above a lift coefficient of about 0.25 and was accompanied by an increased drag rise. These changes are typical of subsonic characteristics of thin highly sweptback wings and are attributed to a leading-edge separation vortex which originates at the apex of the wing, builds up along the leading edge, and trails downstream in a region inboard of the tip, producing flow separation from the wing near the tip. Liquid-film observations on the 60° sweptback wing verify the fact that this vortex flow existed.

In view of the fact that the nonlinearities in the lift and pitching-moment characteristics discussed above are associated with boundary-layer and separation phenomena, an increase in Reynolds number may be expected to reduce the magnitude or delay the occurrence of these nonlinearities.

Effects of Modifications to the 60° Sweptback Wing

Effect of roughness.- To investigate further the nonlinearities observed in the 60° sweptback-wing data, roughness was applied to the leading 10 percent chord of the wing. The results are indicated by the data of figure 12(a). The roughness produced a transition from laminar to turbulent boundary-layer flow which decreased the extent of the trailing-edge separation at low lift coefficients, thus reducing the nonlinearities shown in the basic data. The application of leading-edge roughness did not appreciably affect the characteristics in the high-lift-coefficient range.

Effect of blunt trailing edge.- An alternate method of reducing the laminar separation would be to reduce the adverse pressure gradient through which the boundary layer must flow. An attempt was made to reduce the adverse pressure gradient on the 60° swept wing by building up the airfoil section to the blunt-trailing-edge section shown in figure 8. The effect of this modification, shown by figure 12(b), was to reduce slightly the nonlinearity in the pitching-moment characteristics at low lift coefficients and to delay, to some extent, the onset of tip separation at high lift coefficients. The blunt trailing edge was not as effective, however, as leading-edge roughness in improving the low-lift-coefficient characteristics.

Effect of wing fence.- Low-speed data have shown that considerable improvement to the stability characteristics of sweptback wings at high lifts can be obtained by the use of wing fences. Since the 60° sweptback wing also has a subsonic type of pressure distribution at the test Mach number, a wing fence was indicated as a possible solution to the instability observed at high lift coefficients in the data of figure 11. Consequently, tests were made on the 60° wing with a full-chord fence located on the upper surface of the wing mean aerodynamic chord. The wing-fence data thus obtained (fig. 12(c)) showed considerable improvement in both the stability and the lift-curve-slope characteristics at positive lift coefficients. A lower drag coefficient was also obtained in the high-positive-lift range. These results indicate that the wing fence reduced the intensity of tip separation at the high-positive-lift coefficients by altering the leading-edge separation vortex.

Addition of the wing fence also reduced the nonlinearities in the low-lift range. The improvement observed was greater than that produced by either leading-edge roughness or blunt trailing edge. The fence apparently reduced the trailing-edge separation in the region of the fence at low coefficients by causing transition to a turbulent boundary layer.

Effects of Sweep

The effects of sweep on the aerodynamic characteristics of the wings investigated are summarized in figure 15. The slope measurements made in the determination of the parameters, $C_{L\alpha}$ and y_{cp} , were taken over a lift-coefficient range from -0.2 to 0.2 so that the effects of laminar separation at low lift coefficients would not mask the more fundamental effects of sweep. The values of $\partial C_m / \partial C_L$ are point values measured at the lift coefficients indicated.

The summary includes a comparison of the experimental and theoretical values of lift-curve slope and stability parameter ($\partial C_m / \partial C_L$). The theoretical calculations were for wings of zero thickness.

The theoretical calculations of lift-curve slope for wings with supersonic leading and trailing edges, for wings with subsonic leading edges and supersonic trailing edges, and for wings where the trailing-edge Mach line intersects the leading edge of the wing were made by using references 6 to 8, respectively. For sweep angles for which the trailing-edge Mach line intersects the tip, a straight-line fairing was used to connect the adjacent theoretical values.

To determine the effects of wing flexibility on the aerodynamic characteristics of the wings, static-load tests were made approximating the spanwise and chordwise load distributions indicated by the experimental rolling-moment and pitching-moment results. Corrections to the aerodynamic parameters were determined from the resulting model deflections. The aeroelastic corrections to all of the parameters summarized in figures 15 and 17 except lift-curve slope were found to be either negligible or within the accuracy of experimental determination. The correction to lift-curve slope was determined by considering the angle of attack for a given lift coefficient to be reduced by a weighted average of the twist measured at various spanwise locations during static-load tests. Application of the correction to lift-curve slope resulted in an increase of about 21 percent for the 60° swept wing and smaller increases at lower sweep angles. The corrected lift-curve slopes are indicated on figures 15 and 17 as rigid-wing results.

The values of lift-curve slope generally decreased with increasing sweep angle. For all sweep angles, the experimental values of lift-curve slope were found to be less than those predicted by theory, with the greatest difference occurring at the sweep angle where the Mach lines were parallel to the leading edge of the wing. Results of tests of an extensive series of triangular wings reported in reference 9 showed a similar relationship between the experimental and theoretical lift-curve slopes.

Comparison of the theoretical and experimental values of $\partial C_m / \partial C_L$ are presented in figure 15. The experimental values given up to 45° sweep were measured at lift coefficients of 0 and 0.5 to indicate the effect on longitudinal stability of the laminar separation previously discussed. At the higher lift coefficient where the separation effects were minimized, good agreement between experimental and theoretical values was obtained. The experimental data for the 60° wing are not presented because the fundamental sweep effects are masked by the severe separation occurring on this wing.

The variations with sweep angle of $\partial C_m / \partial C_L$ and the lateral center of pressure y_{cp} presented in figure 15 indicate a small spanwise shift of the center of lifting pressure without appreciably affecting the aerodynamic center for sweep angles up to 45° .

The variation with sweep angle of the drag coefficient at zero lift presented in figure 15 illustrates that practically no reduction in zero-lift drag resulted as the sweep angle was increased from 0° to 35° . With further increases in sweep, however, a significant reduction in drag was observed as a result of the loss of pressure drag occurring as the chordwise pressure distributions changed from the supersonic to the subsonic type. The values of zero-lift drag coefficient presented for the wings alone included the end-plate drag. A test of the 45° swept wing without end plate and with the root gap sealed indicated that the end-plate drag coefficient was about 0.002 for this wing.

The reduction of zero-lift drag coefficient observed is reflected directly in the increase in lift-drag ratio as the wings were swept behind the Mach lines (fig. 16). Values of $(L/D)_{max}$ for wings alone increased from 5.0 to 8.7 as the sweep angle was increased from 35° to 60° (fig. 15). The lift-drag ratios are also influenced by the drag-rise factor $\Delta C_D / C_L^2$, values of which are presented in figure 17. The measured values represent the drag-rise factor at low lift coefficients. The 60° swept wing, for example, exhibited considerably higher values of drag-rise factor at lift coefficients above about 0.25. The results indicate that a significant reduction in drag-rise factor was observed as the sweep angle was increased from 45° to 60° .

Examination of theoretical values of drag-rise factor is of value in interpreting the experimental results. For wings with supersonic leading edges, the lifting pressures are directed normal to the wing chord. Thus for small angles, the drag due to lift is equal to the lift multiplied by the angle of attack. The resulting drag-rise factor is the reciprocal of the lift-curve slope. For wings with subsonic leading edges, the drag-rise factor is the reciprocal of the lift-curve slope reduced by the amount of the leading-edge suction. Theoretical values of leading-edge suction were determined by the methods of reference 8.

In the experimental results, if the assumption is made that the viscous drag is independent of angle of attack, the amount of leading-edge suction actually realized is indicated by the difference between the observed drag-rise factor and the reciprocal of the lift-curve slope. The lift-curve slope of the rigid wing must be used so that the angle of attack adequately represents the inclination of the lifting pressures. The validity of the assumption of constant viscous drag is indicated by the agreement between the drag-rise factor and the lift-curve-slope reciprocal at low sweep angles for which the leading-edge suction would be expected to be zero. Thus, the results indicate that the 60° swept wing experienced a significant proportion of the theoretically available leading-edge suction. Comparison of the theoretical and experimental data of figure 17 shows fair agreement of the trends of the drag-rise variation with sweep angle. The displacement between the curves is a result of the disagreement between the experimental and theoretical values of lift-curve slope.

Effects of Fuselage

Comparison of the data of figures 11 and 13 indicates that addition of the fuselage considerably reduced the nonlinearities shown for the wing alone. In the very low angle-of-attack range, the influence of the fuselage on the wing apparently was such as to produce conditions less favorable to laminar separation. At the higher angles of attack and high sweep angles the fuselage evidently reduced the effect of the leading-edge separation vortex, materially improving the lift-curve slope and longitudinal stability characteristics for the 60° sweptback wing.

Examination of figure 15 indicates that at sweep angles below 45°, addition of the fuselage produced a small increase in lift-curve slope and forward movement of the aerodynamic center at a lift coefficient of 0.5.

The observed increases in C_{D_0} and decreases in $(L/D)_{max}$ resulting from addition of the fuselage should be interpreted with caution because the tunnel-wall boundary layer would be expected to have considerable effect on the fuselage pressure distribution and base drag.

CONCLUSIONS

Tests were conducted at a Mach number of 1.38 and a Reynolds number of 390,000 to determine the supersonic aerodynamic characteristics of a

series of sweptback wings and wing-body configurations. The test results are summarized in the following conclusions:

1. At the Reynolds number of the present tests, laminar separation occurred on the rear portions of the wings at all sweep angles producing reduced stability at lift coefficients below 0.1.
2. Increasing the angle of sweepback resulted in a reduction in lift-curve slope and zero-lift drag coefficient, an increase in maximum lift-drag ratio, and an outward movement of the lateral center of pressure.
3. The experimental lift-curve slopes were in all cases less than those predicted from linearized theory, the maximum discrepancy occurring at the sweep angle for which the Mach lines were parallel to the leading edge.
4. Good agreement between theoretical and experimental aerodynamic-center locations was observed at sweep angles up to 45° for lift coefficients at which laminar separation effects were not observed.
5. A leading-edge separation vortex occurred on the 60° swept wing at lift coefficients above 0.25, producing severe instability and a large drag increase. At lift coefficients below 0.25, however, this wing exhibited a considerable proportion of the theoretically available leading-edge suction.
6. The effects of laminar separation at low lift coefficients on the 60° swept wing were significantly reduced by the use of leading-edge roughness, a thickened trailing edge, or an upper-surface fence. The fence also considerably reduced the instability occurring at the higher lift coefficients.

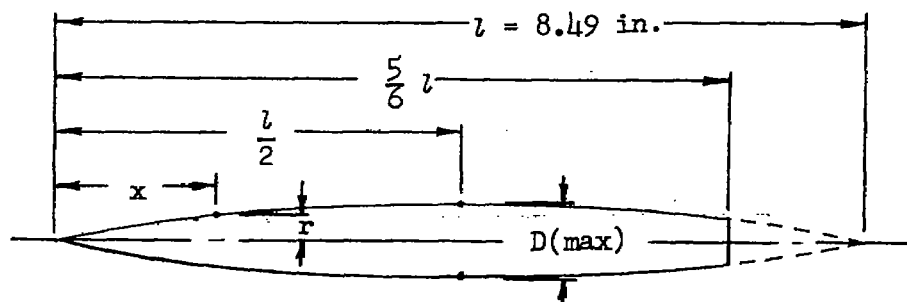
Langley Aeronautical Laboratory
National Advisory Committee for Aeronautics
Langley Air Force Base, Va.

REFERENCES

1. Goodson, Kenneth W., and Morrison, William D., Jr.: Aerodynamic Characteristics of a Wing with Unswept Quarter-Chord Line, Aspect Ratio 4, Taper Ratio 0.6, and NACA 65A006 Airfoil Section. Transonic-Bump Method. NACA RM L9H22, 1949.
2. Sleeman, William C., Jr., and Becht, Robert E.: Aerodynamic Characteristics of a Wing with Quarter-Chord Line Swept Back 35° , Aspect Ratio 4, Taper Ratio 0.6, and NACA 65A006 Airfoil Section. Transonic-Bump Method. NACA RM L9B25, 1949.
3. Weil, Joseph, and Goodson, Kenneth W.: Aerodynamic Characteristics of a Wing with Quarter-Chord Line Swept Back 45° , Aspect Ratio 4, Taper Ratio 0.6, and NACA 65A006 Airfoil Section. Transonic-Bump Method. NACA RM L9A21, 1949.
4. King, Thomas J., Jr., and Myers, Boyd C., II: Aerodynamic Characteristics of a Wing with Quarter-Chord Line Swept Back 60° , Aspect Ratio 4, Taper Ratio 0.6, and NACA 65A006 Airfoil Section. Transonic-Bump Method. NACA RM L9G27, 1949.
5. Madden, Robert T.: Aerodynamic Study of a Wing-Fuselage Combination Employing a Wing Swept Back 63° . Characteristics at a Mach Number of 1.53 Including Effect of Small Variations of Sweep. NACA RM A8J04, 1949.
6. Harmon, Sidney M., and Jeffreys, Isabella: Theoretical Lift and Damping in Roll of Thin Wings with Arbitrary Sweep and Taper at Supersonic Speeds. Supersonic Leading and Trailing Edges. NACA TN 2114, 1950.
7. Malvestuto, Frank S., Jr., Margolis, Kenneth, and Ribner, Herbert S.: Theoretical Lift and Damping in Roll of Thin Sweptback Wings of Arbitrary Taper and Sweep at Supersonic Speeds. Subsonic Leading Edges and Supersonic Trailing Edges. NACA TN 1860, 1949.
8. Cohen, Doris: Formulas and Charts for the Supersonic Lift and Drag of Flat Swept-Back Wings with Interacting Leading and Trailing Edges. NACA TN 2093, 1950.
9. Love, Eugene S.: Investigations at Supersonic Speeds of 22 Triangular Wings Representing Two Airfoil Sections for Each of 11 Apex Angles. NACA RM L9D07, 1949.

TABLE I.- FUSELAGE ORDINATES

[Basic fineness ratio 12; actual fineness ratio 10 achieved by cutting off the rear one-sixth of the body; $\bar{c}/4$ located at $l/2$]



Ordinates			
x/l	r/l	x/l	r/l
0	0	0	0
.005	.00231	.4500	.04113
.0075	.00298	.5000	.04167
.0125	.00428	.5500	.04130
.0250	.00722	.6000	.04024
.0500	.01205	.6500	.03842
.0750	.01613	.7000	.03562
.1000	.01971	.7500	.03128
.1500	.02593	.8000	.02526
.2000	.03090	.8338	.02000
.2500	.03465	.8500	.01852
.3000	.03741	.9000	.01125
.3500	.03933	.9500	.00439
.4000	.04063	1.0000	0

L. E. radius = 0.0005l

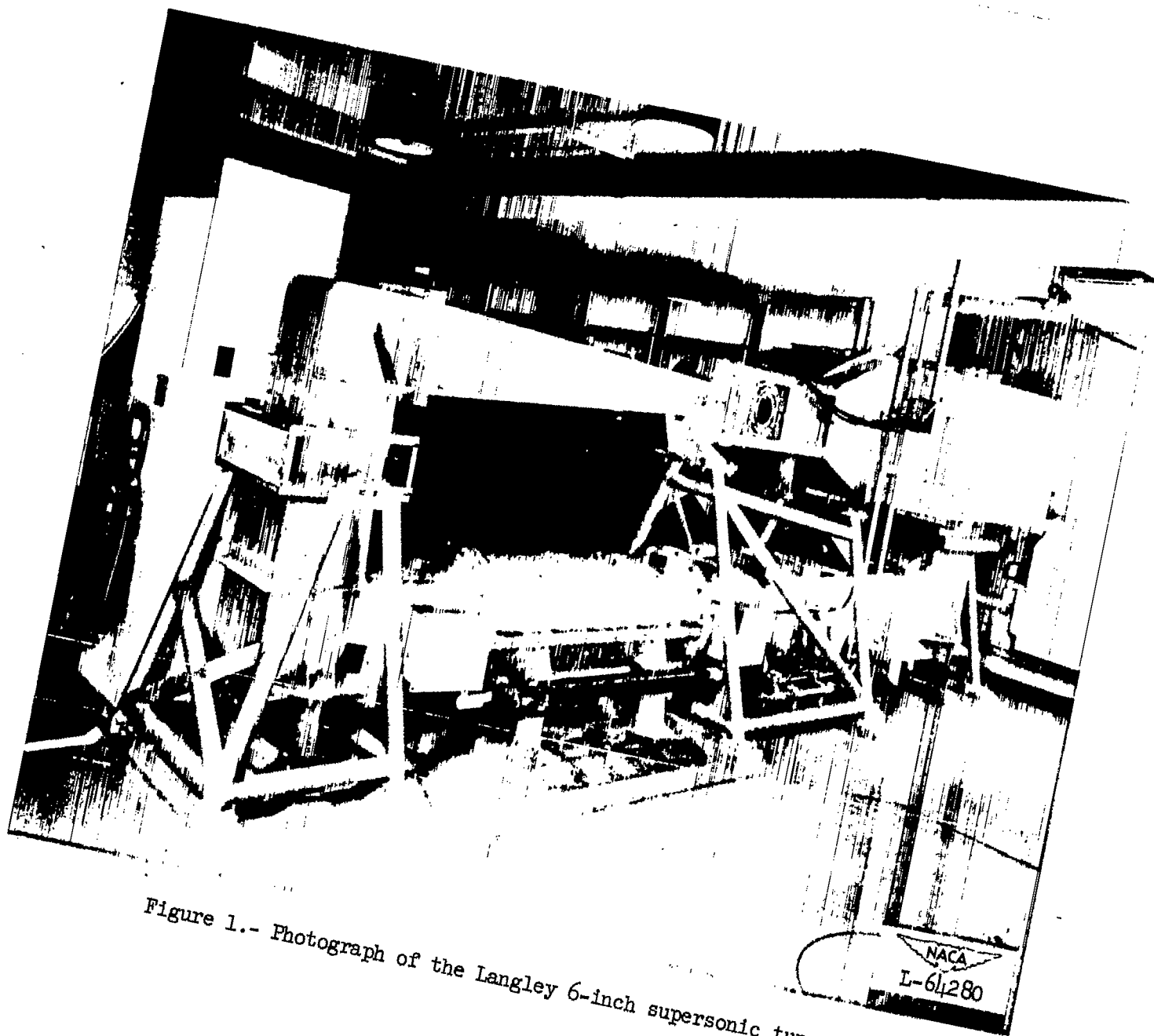


Figure 1.- Photograph of the Langley 6-inch supersonic tunnel.



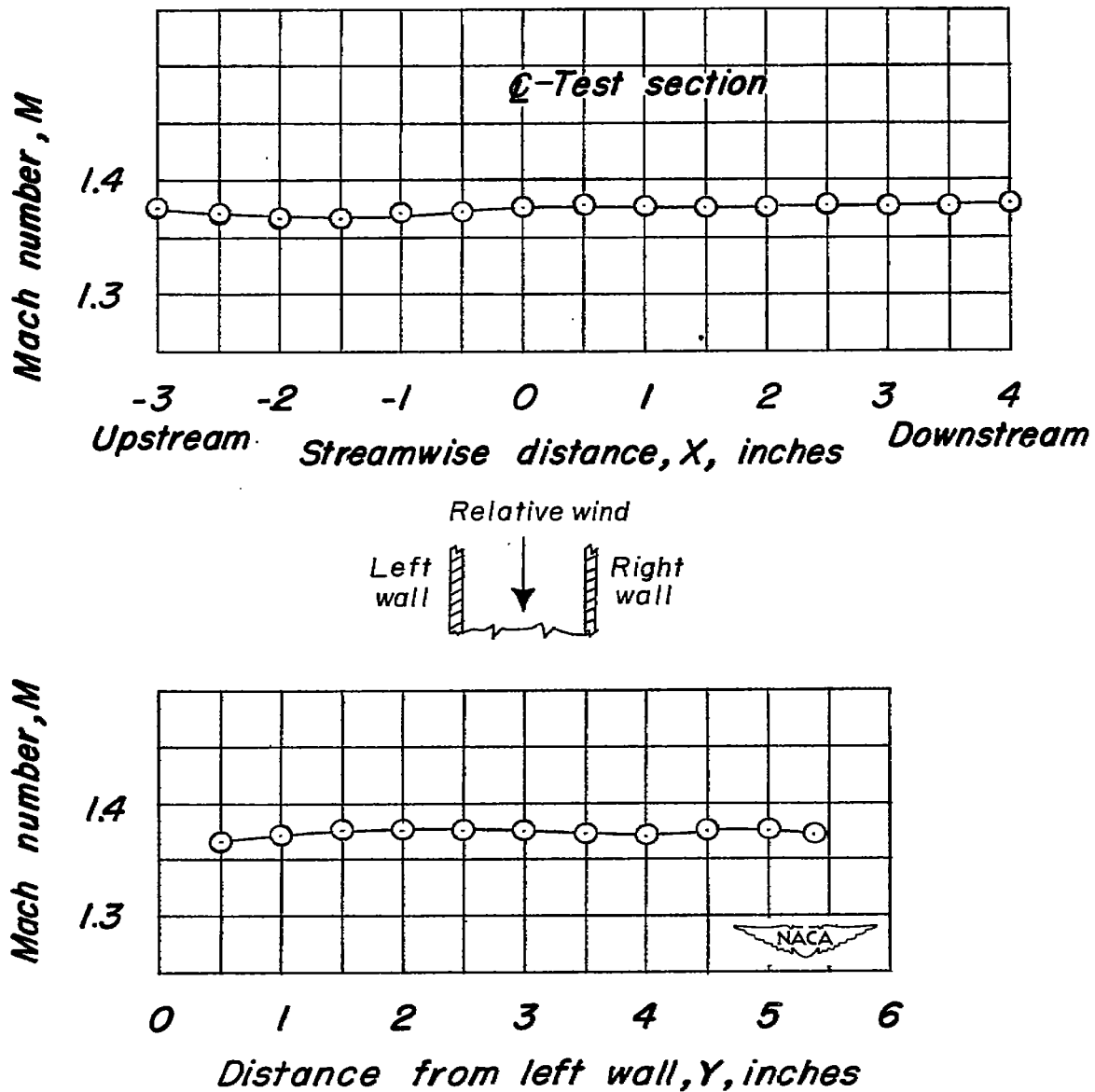


Figure 2.- Mach number variation measured along the test-section center lines of the Langley 6-inch supersonic tunnel.

○ 3 inches ahead of test section \mathcal{C}

△ 1/2 inches behind test section \mathcal{C}

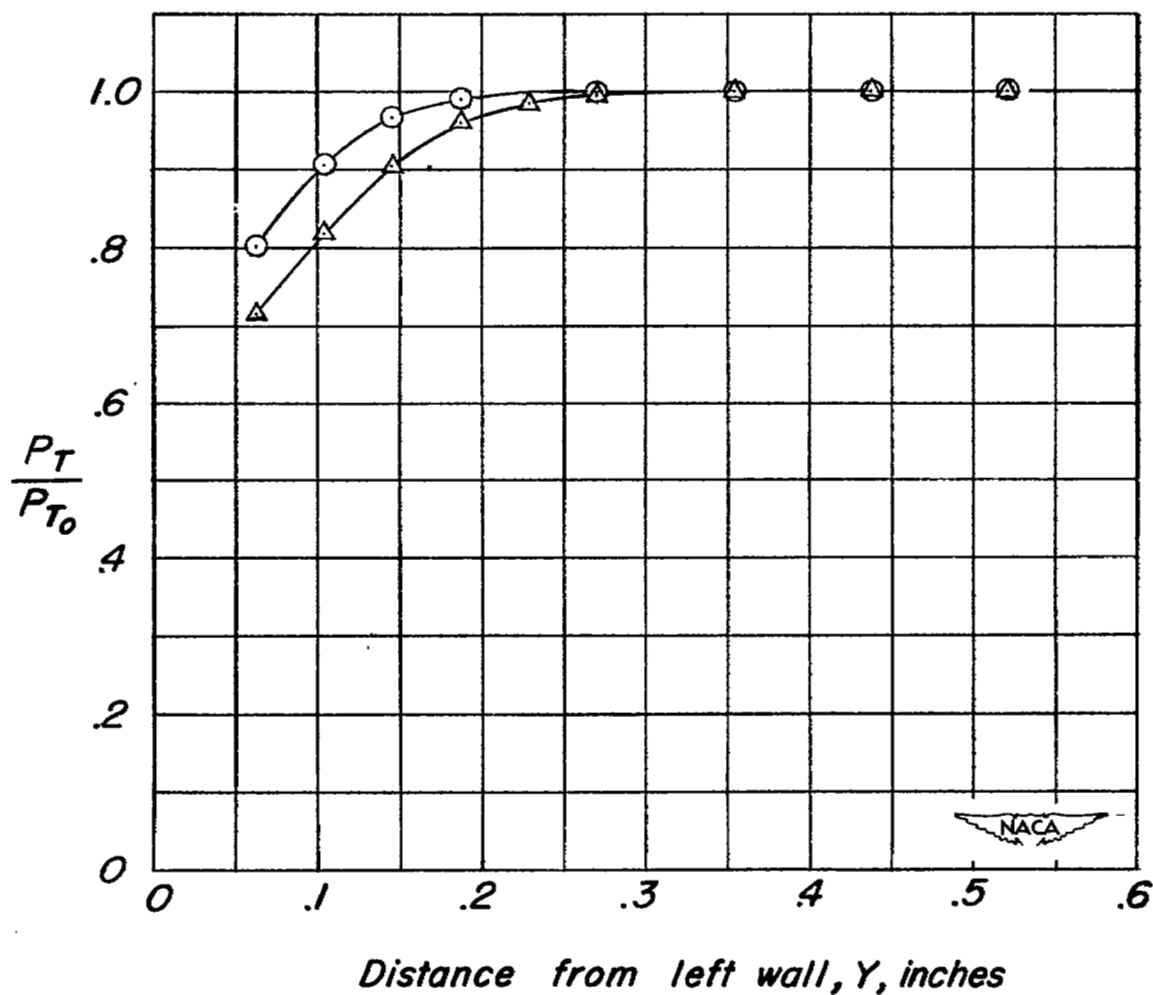


Figure 3.- Tunnel-wall boundary-layer survey measured in horizontal center plane of the Langley 6-inch supersonic tunnel.

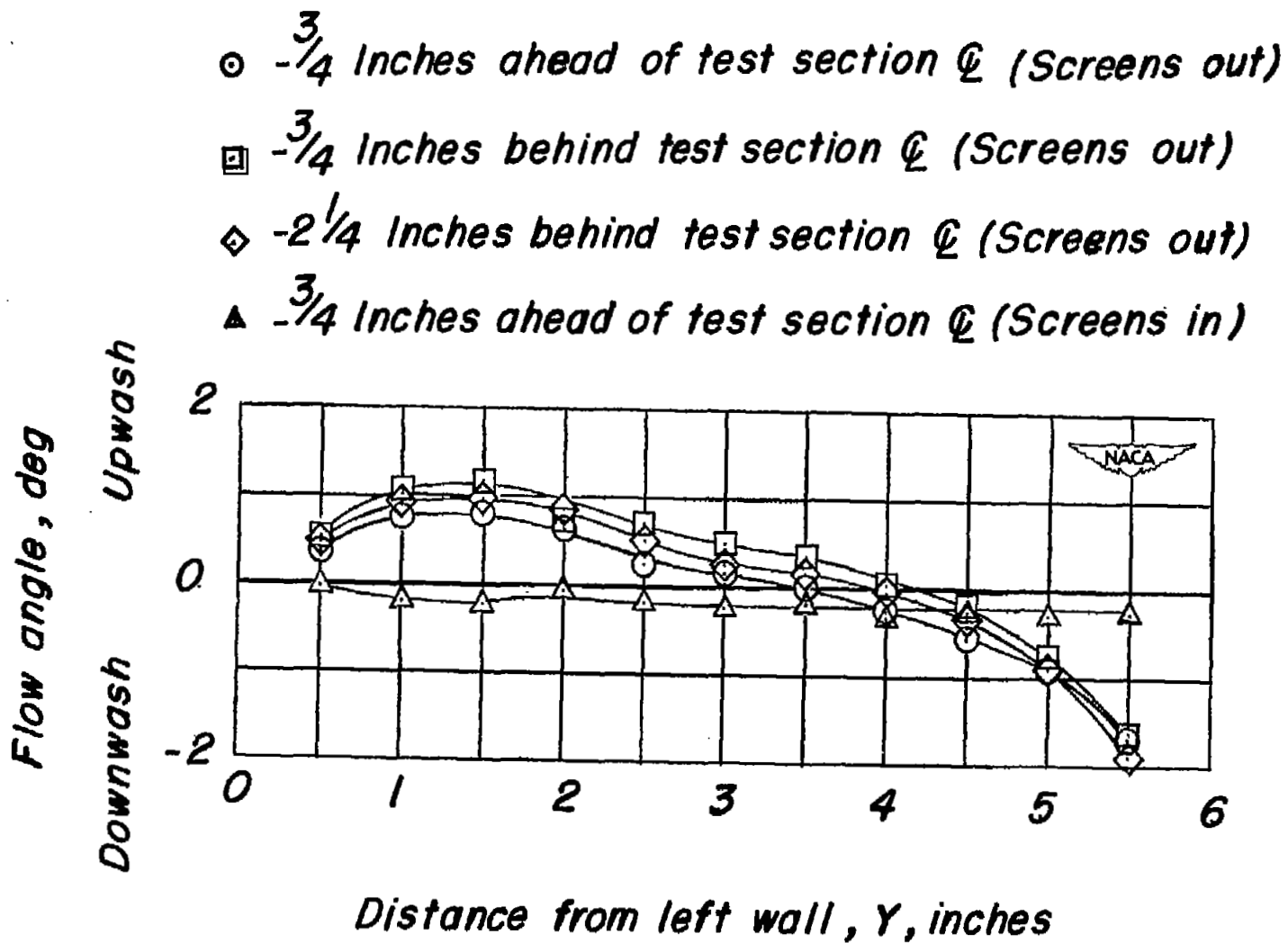


Figure 4.- Spanwise variation of flow alignment angle measured in the horizontal center plane of the Langley 6-inch supersonic tunnel.



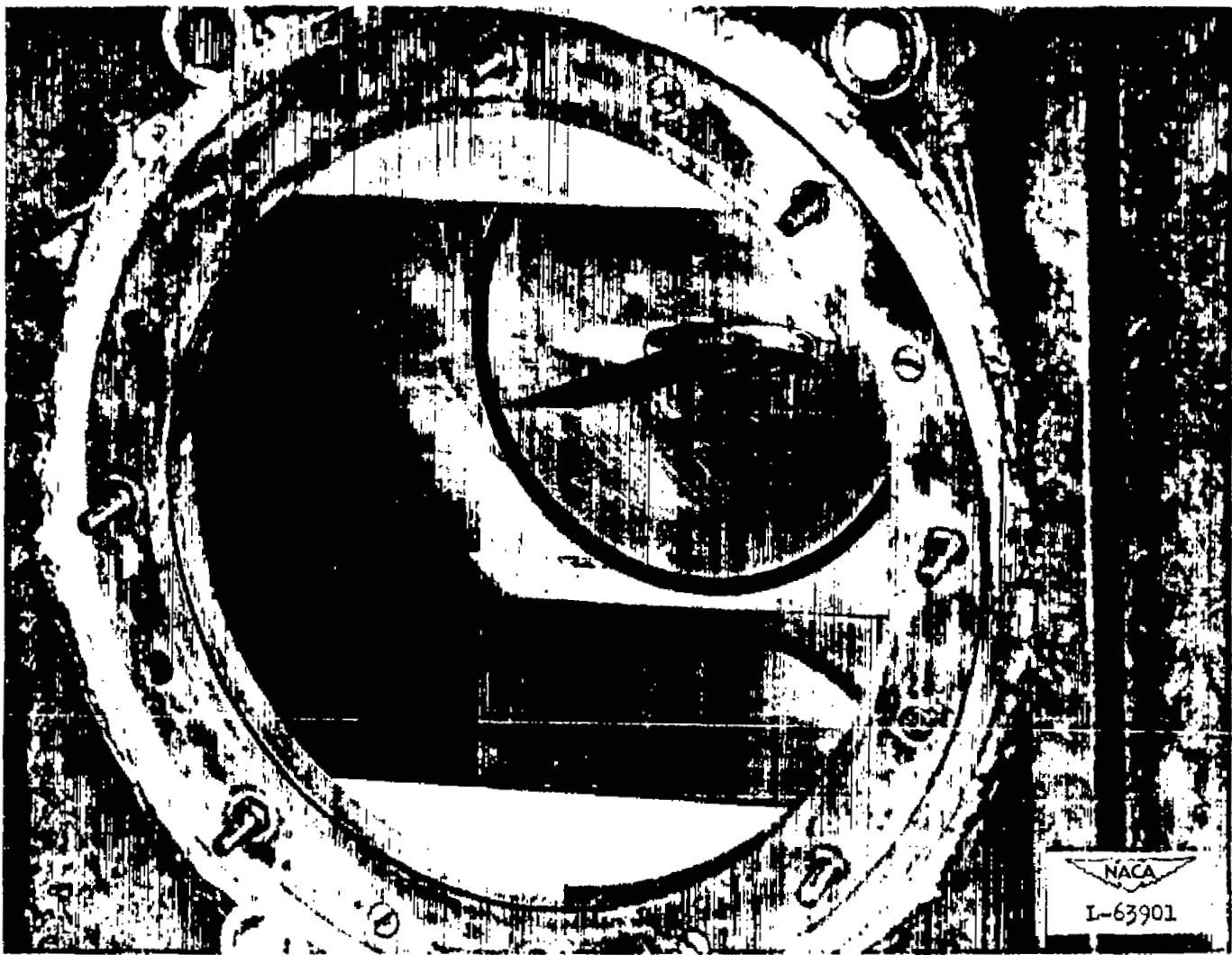
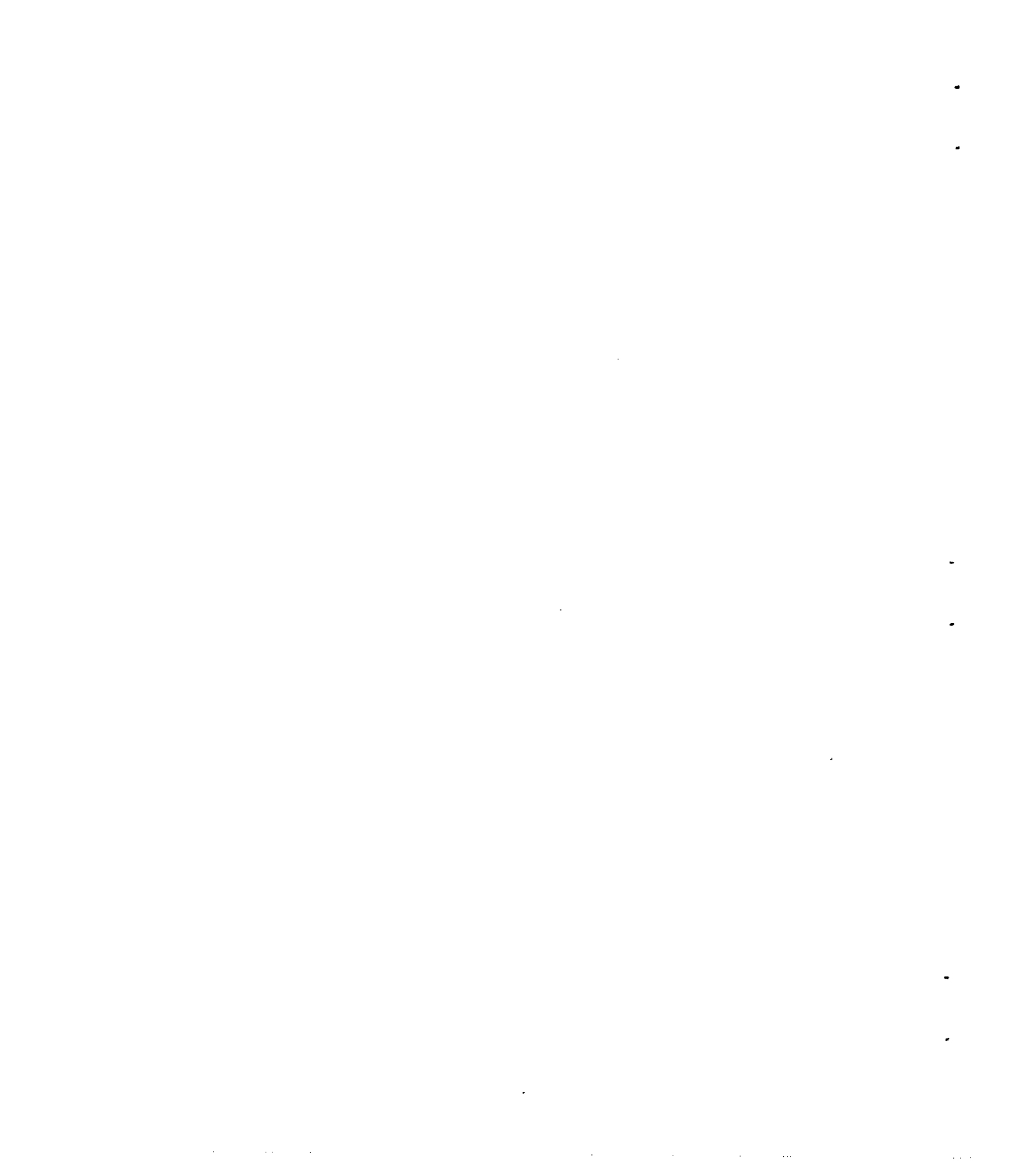


Figure 5.- Photograph showing typical model installation in the Langley 6-inch supersonic tunnel.



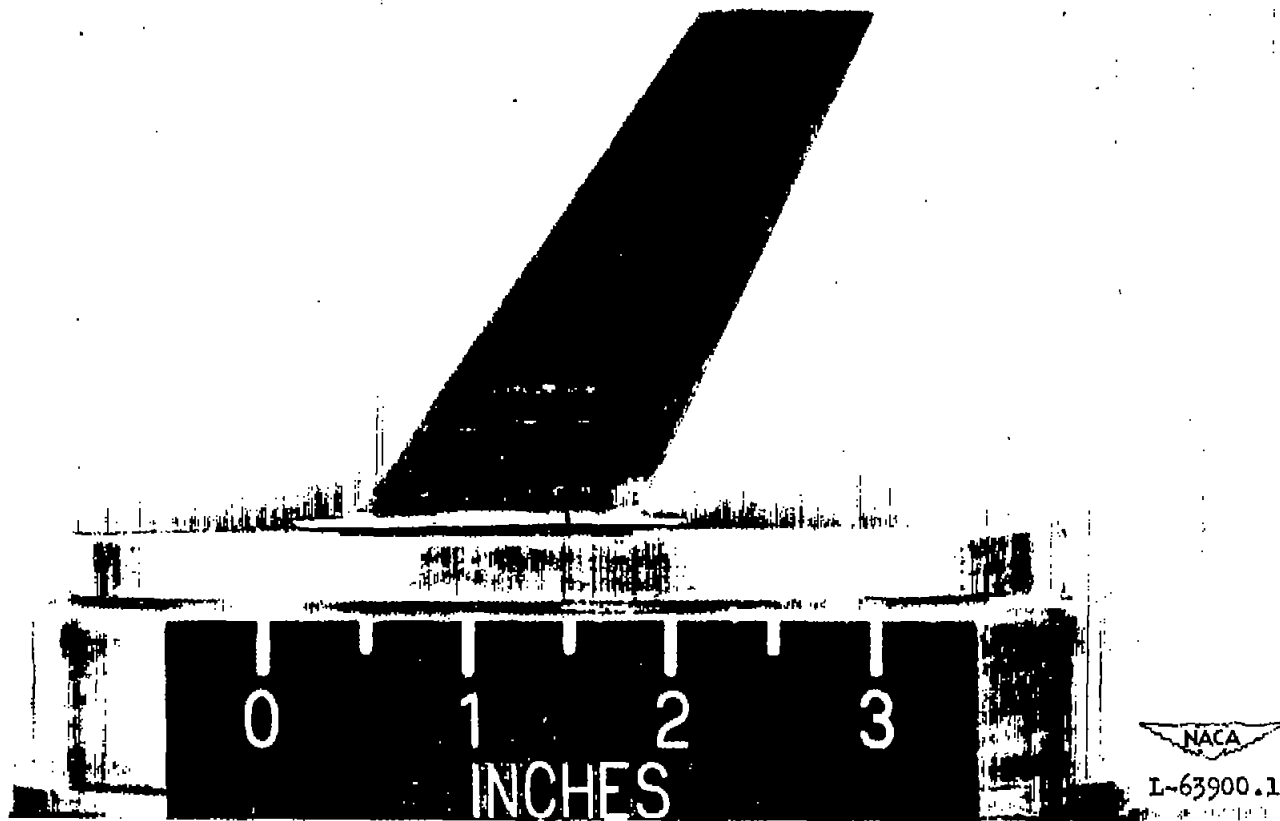
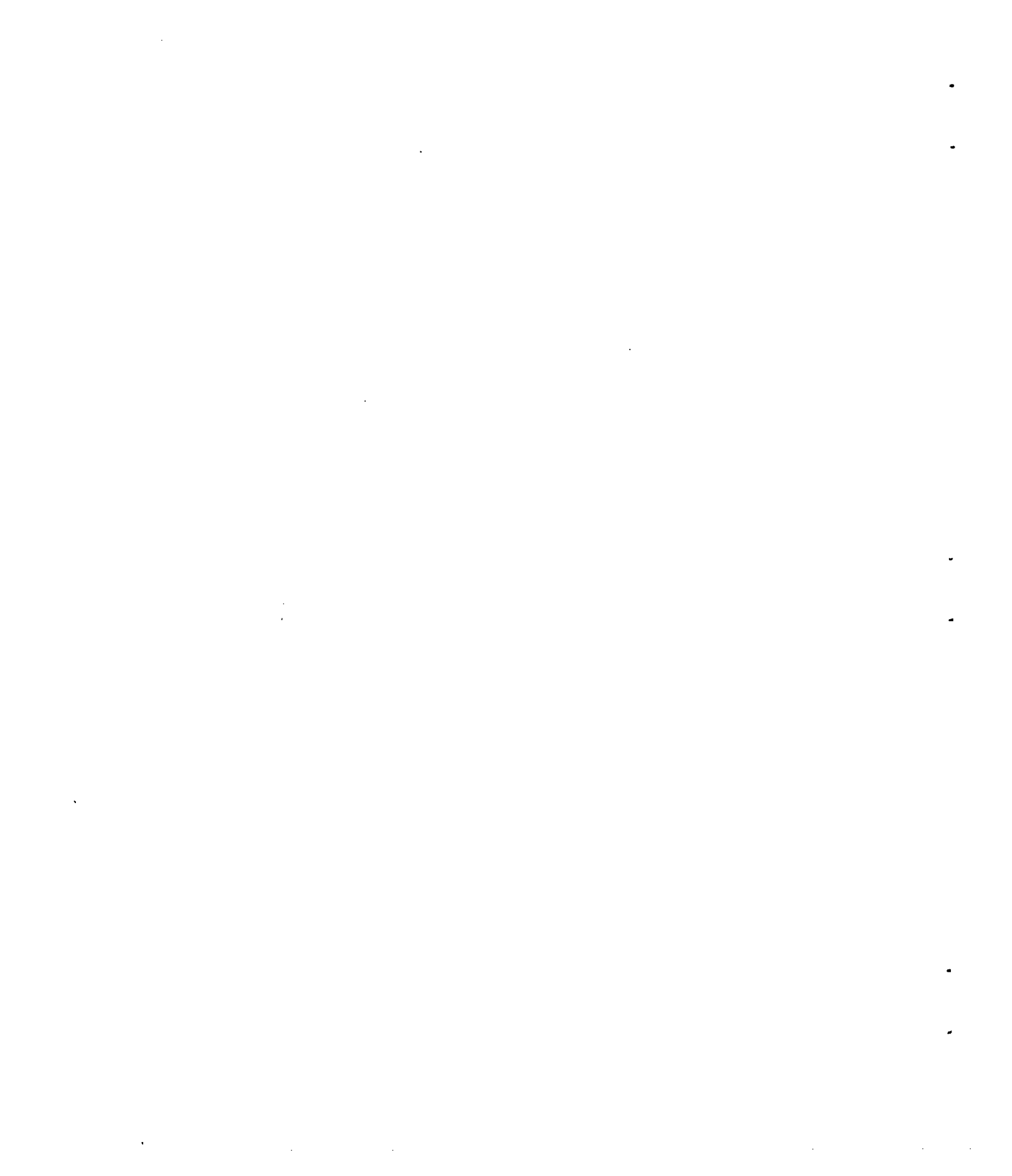


Figure 6.- Photograph of a typical model mounted on the balance turntable.



Tabulated wing data
 Area (twice semispan)
 Mean aerodynamic chord
 Aspect ratio
 Taper ratio
 Incidence
 Dihedral
 Airfoil section parallel to
 free stream

0.045 sq. ft.
 1.3 in.
 4.0
 0.6
 0.0°
 0.0°
 NACA 65A006

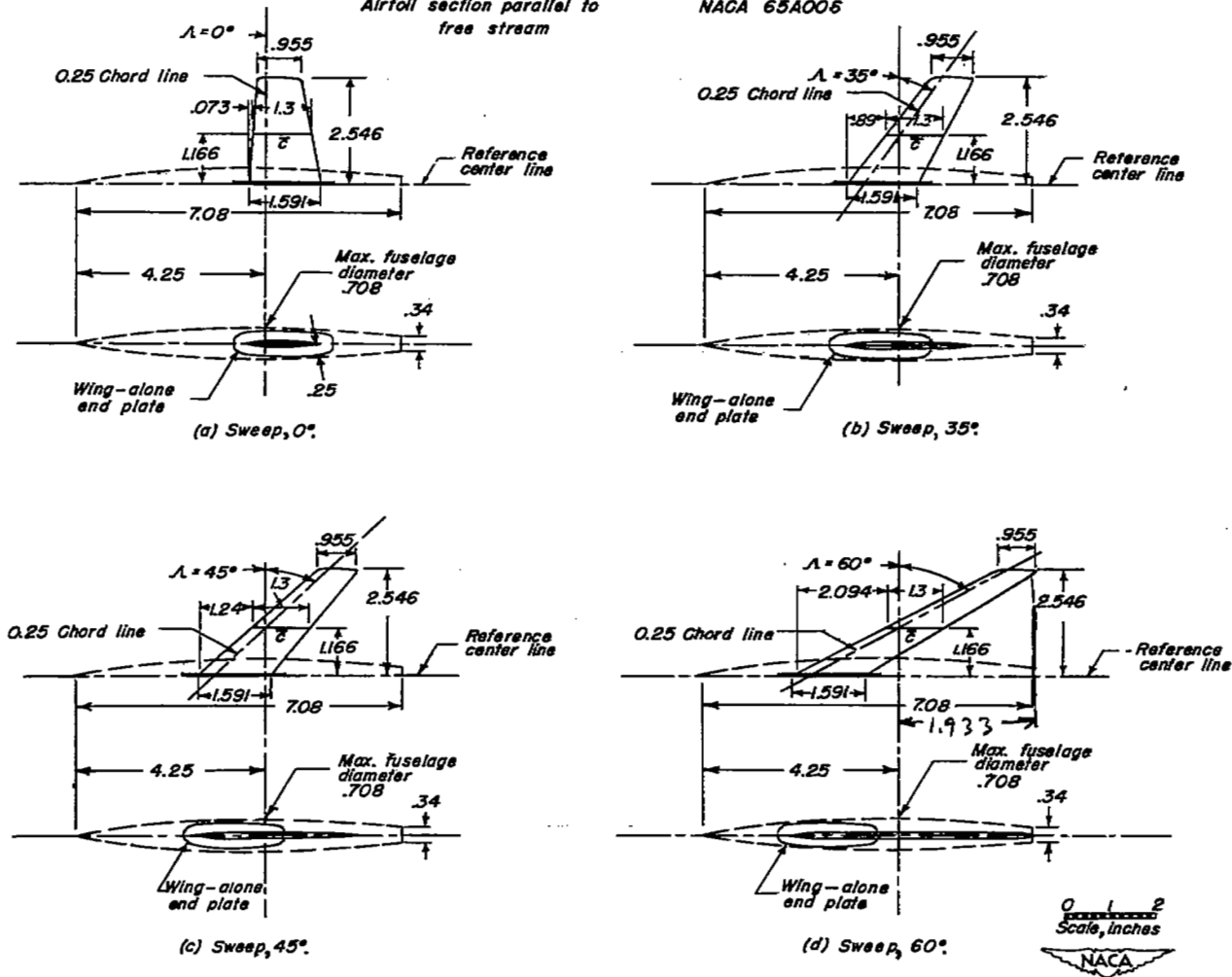


Figure 7.- Geometric details of a series of sweptback wings having an aspect ratio of 4, taper ratio of 0.6, and an NACA 65A006 airfoil section.

Handwritten notes:
 $\frac{1.3}{11} = 0.118$
 2.094
 1.24
 2.14

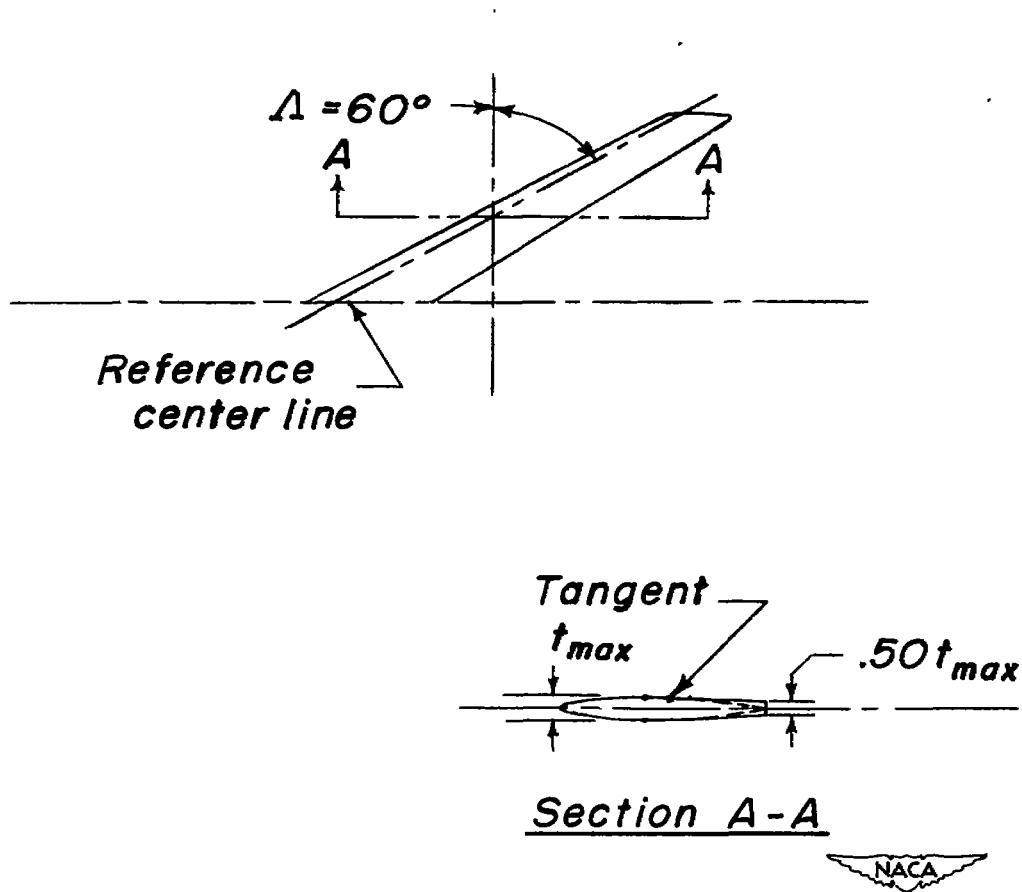


Figure 8.- Details of blunt trailing edge on wing having 60° sweep, aspect ratio 4, taper ratio 0.6, and NACA 65A006 airfoil section.

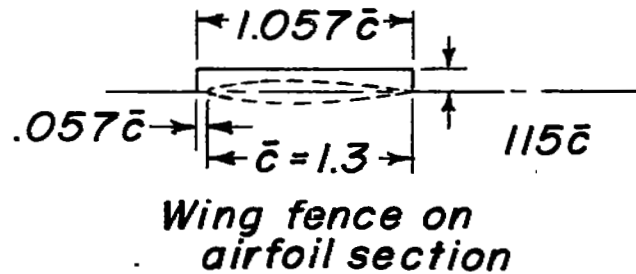
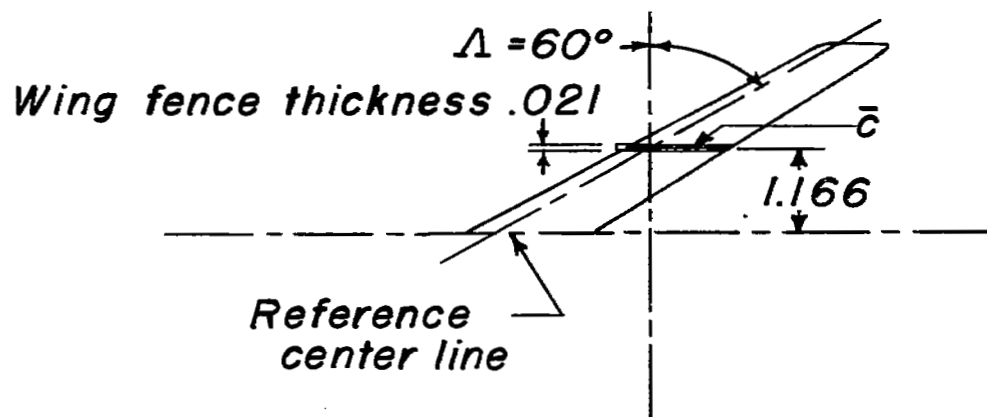


Figure 9.- Details of wing fence on wing having 60° sweep, aspect ratio 4, taper ratio 0.6, and NACA 65A006 airfoil section.

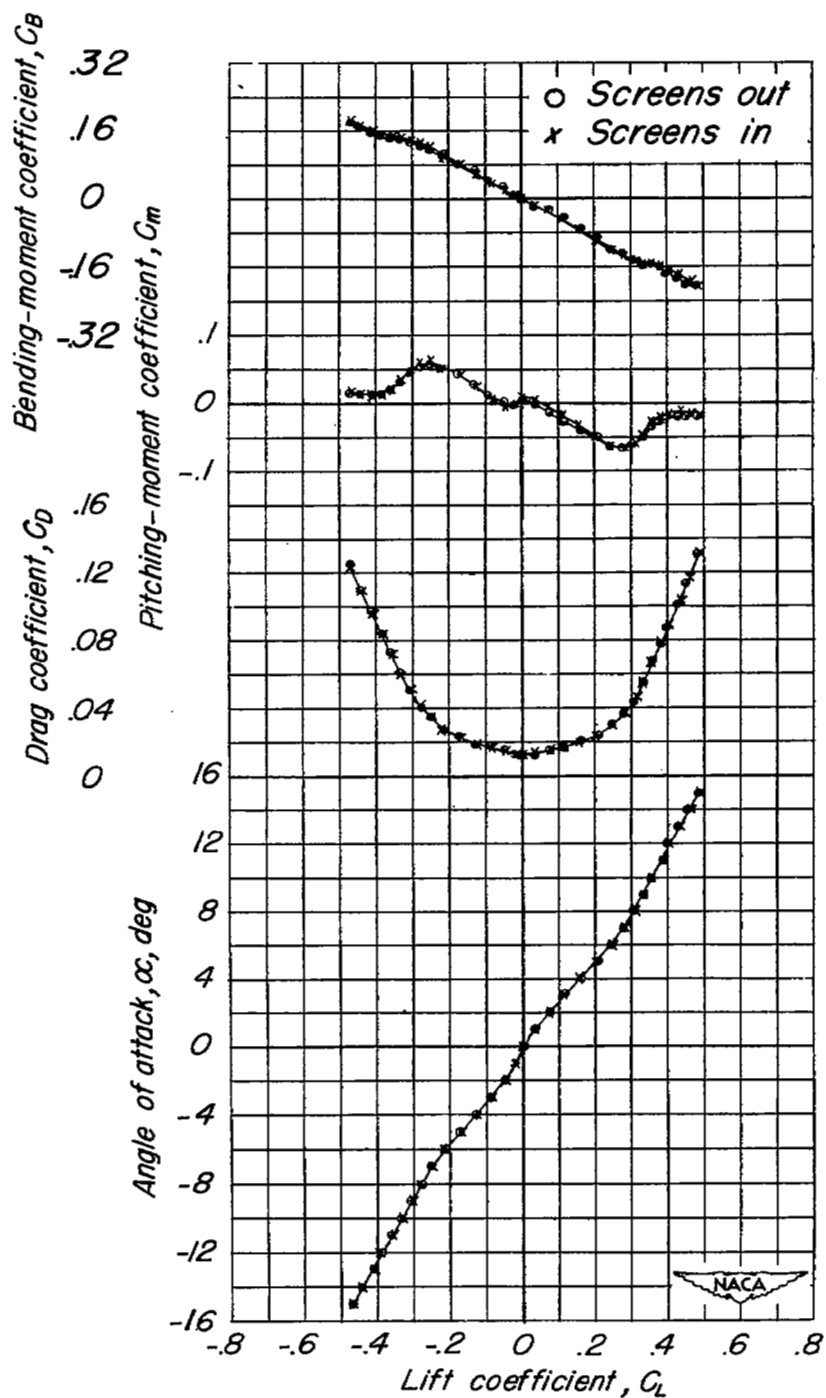
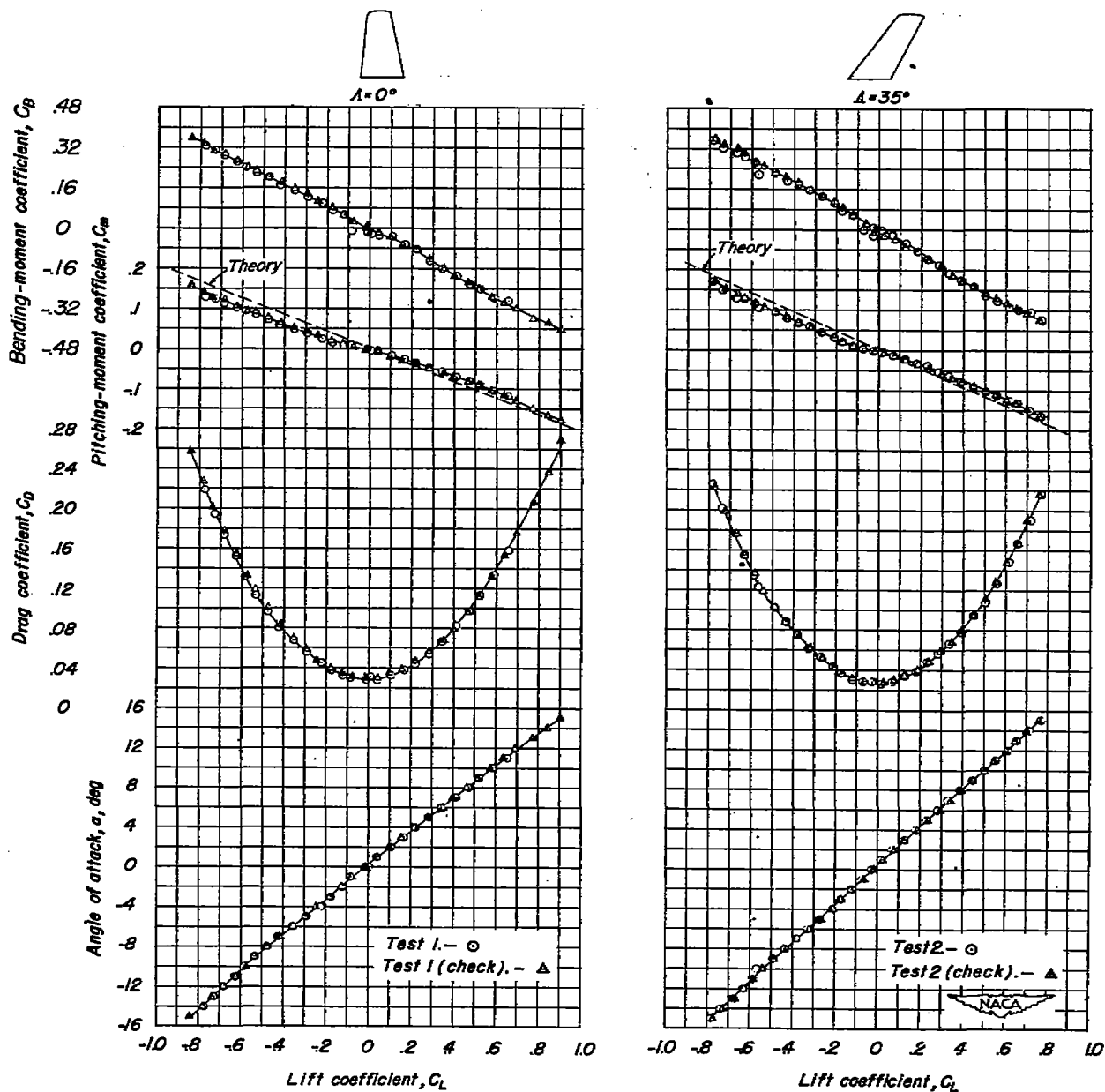
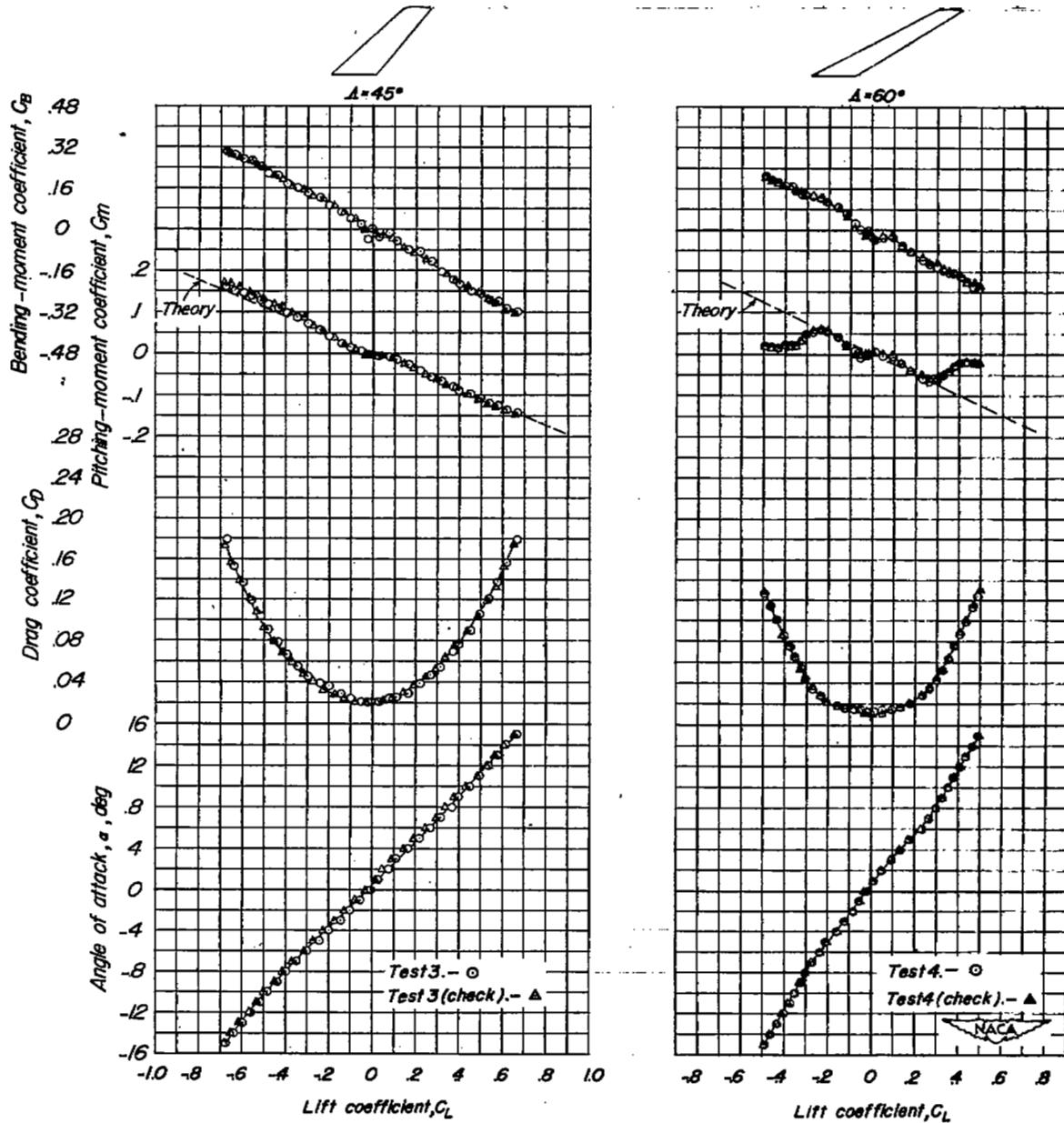


Figure 10.- Effect of screen installation on the aerodynamic characteristics of the 60° sweptback wing as tested in the Langley 6-inch supersonic tunnel.



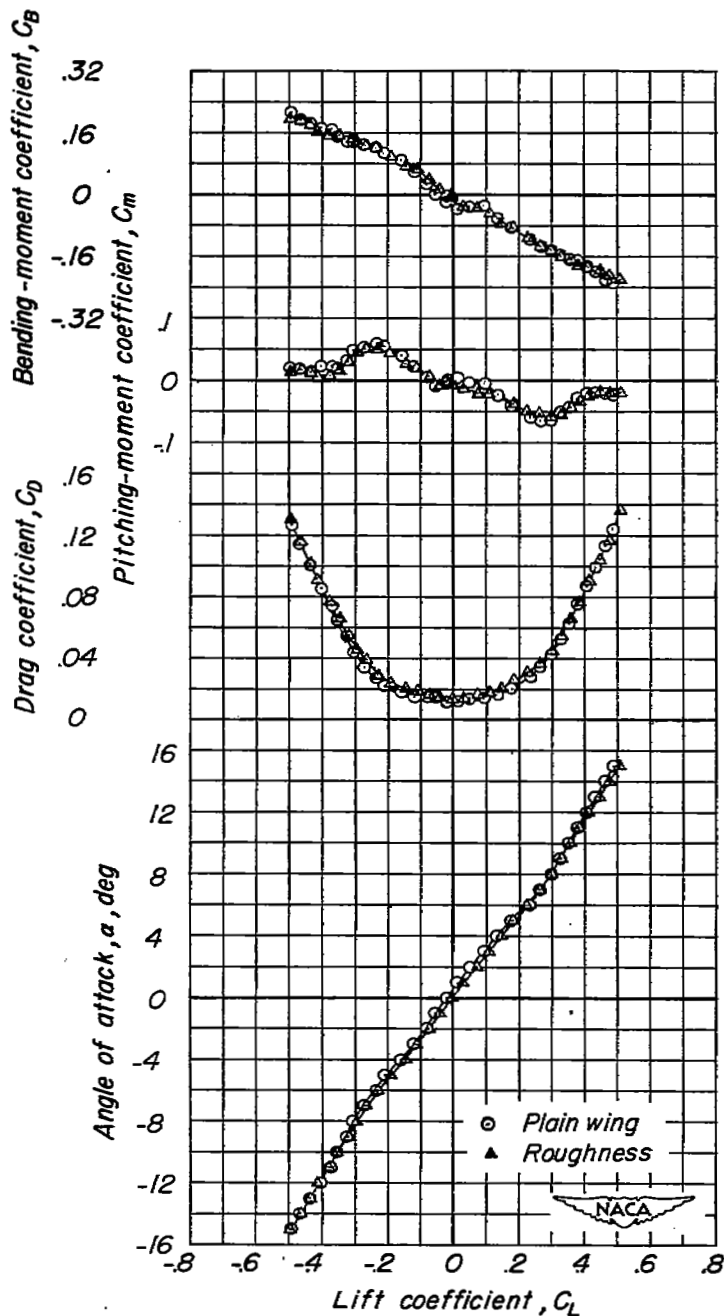
(a) $\Lambda = 0^\circ, 35^\circ$.

Figure 11.- Wing-alone data for a series of sweptback wings having an aspect ratio 4, taper ratio 0.6, and NACA 65A006 airfoil section.



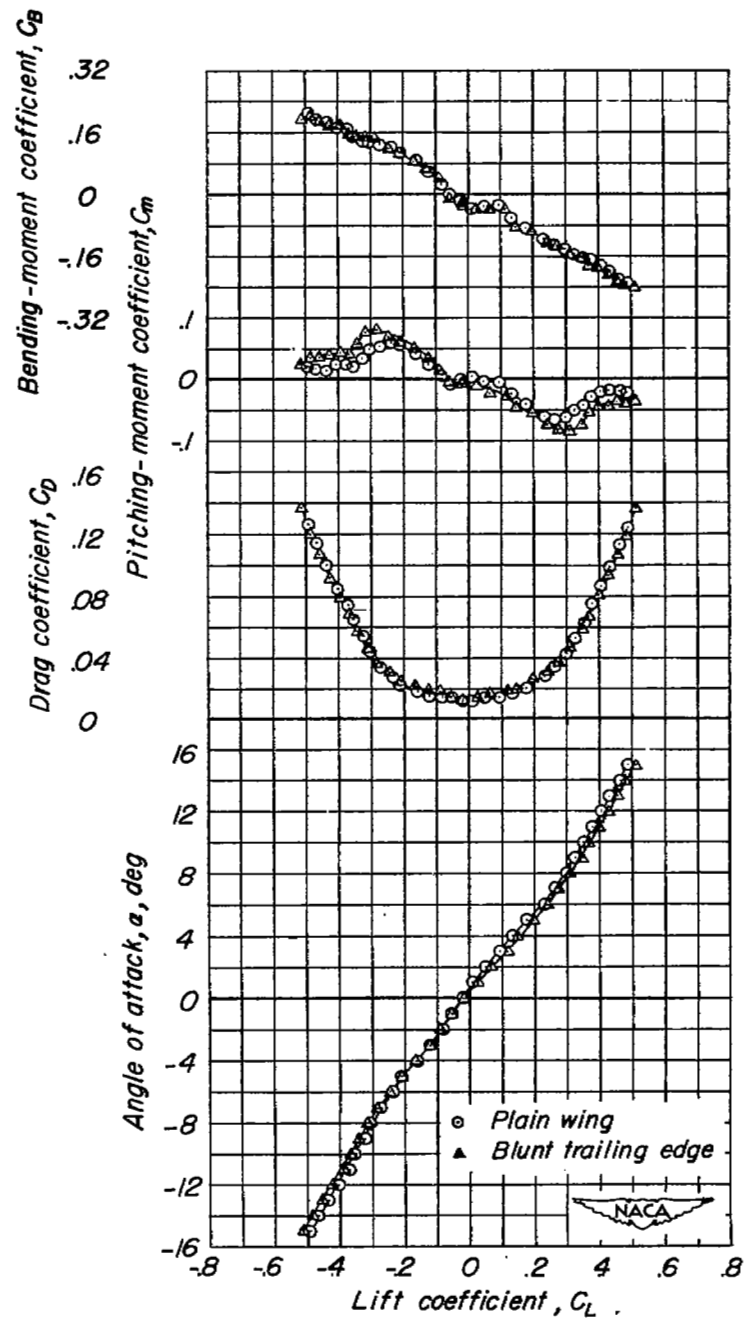
(b) $\Lambda = 45^\circ, 60^\circ$.

Figure 11.- Concluded.



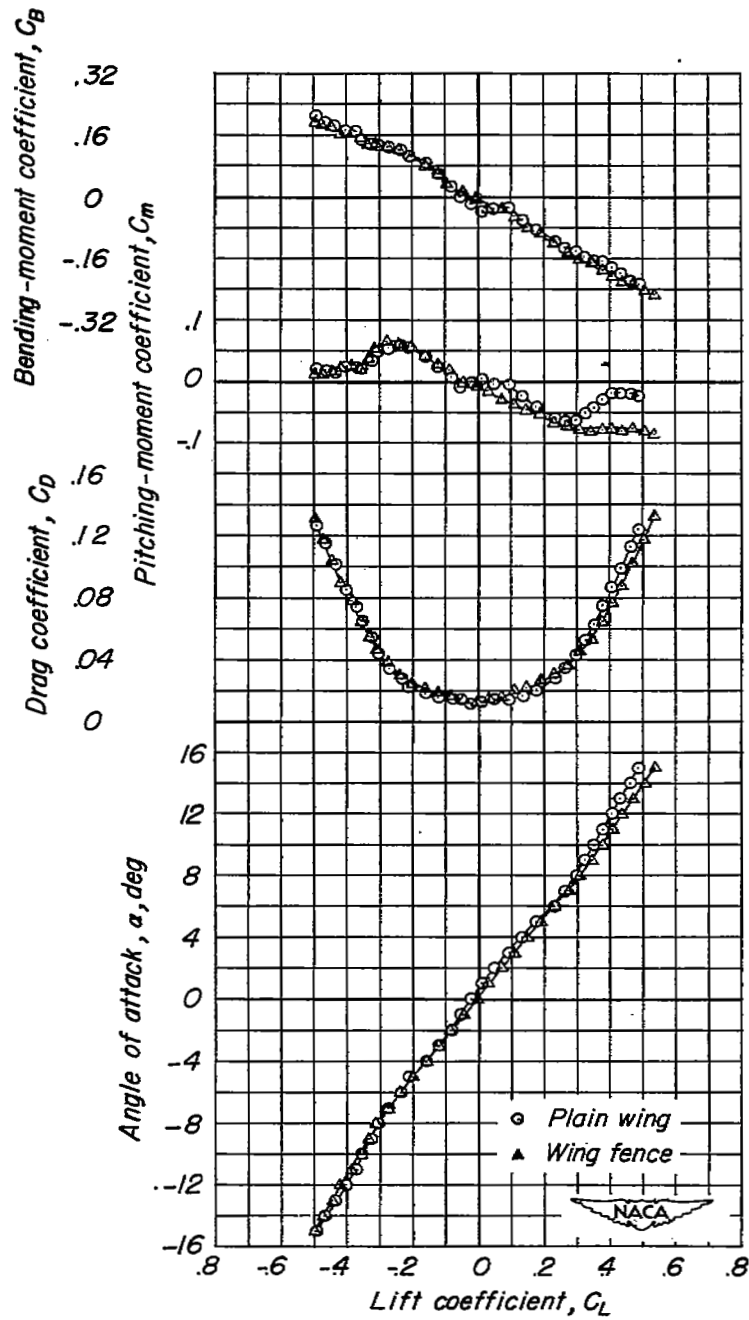
(a) Effect of roughness.

Figure 12.- Effects of roughness, blunt trailing edge, and wing fence on the wing-alone aerodynamic characteristics for a model with 60° swept-back wing, aspect ratio 4, taper ratio 0.6, and NACA 65A006 airfoil section.



(b) Effect of blunt trailing edge.

Figure 12.- Continued.



(c) Effect of wing fence.

Figure 12.- Concluded.

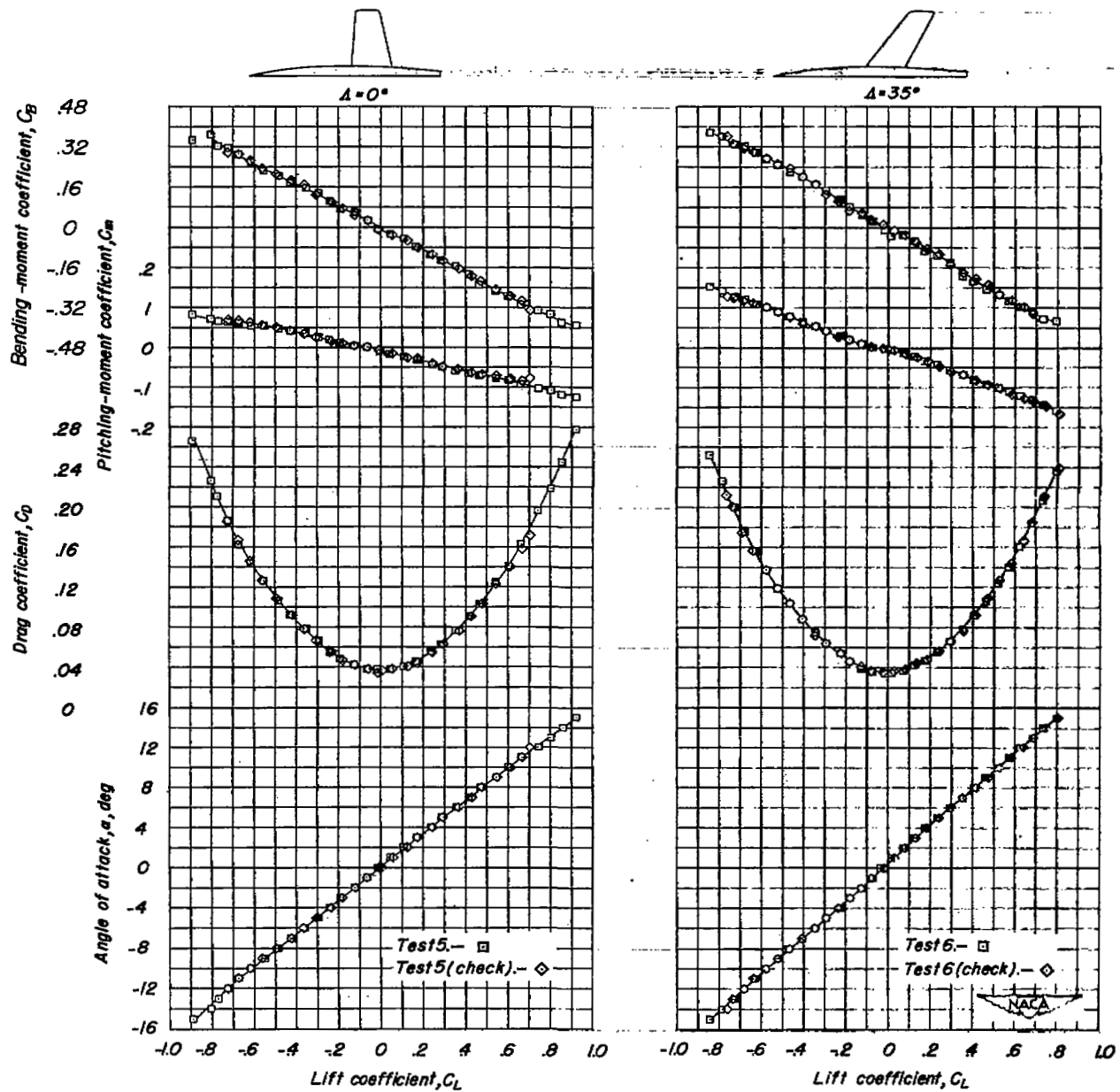
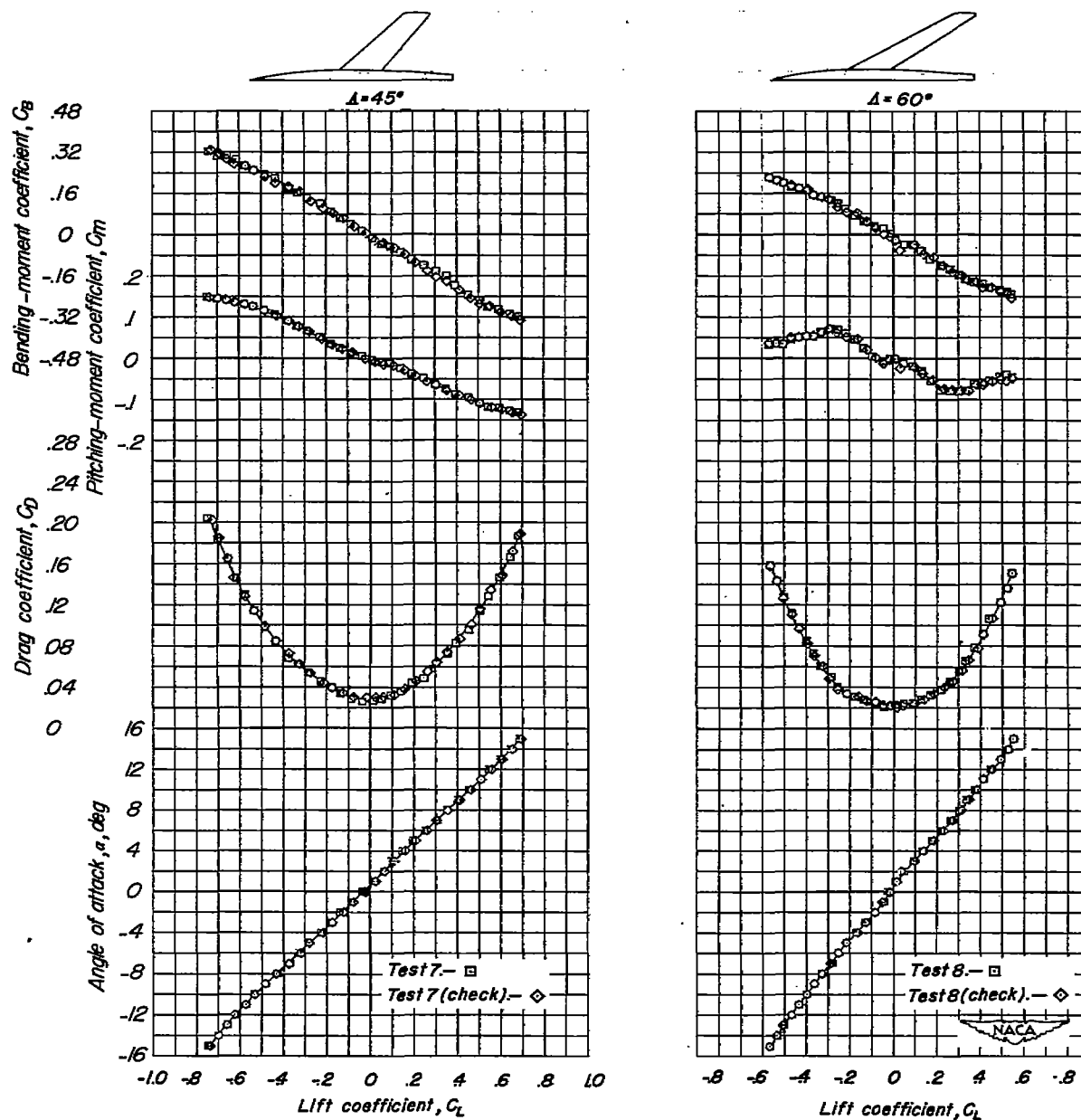
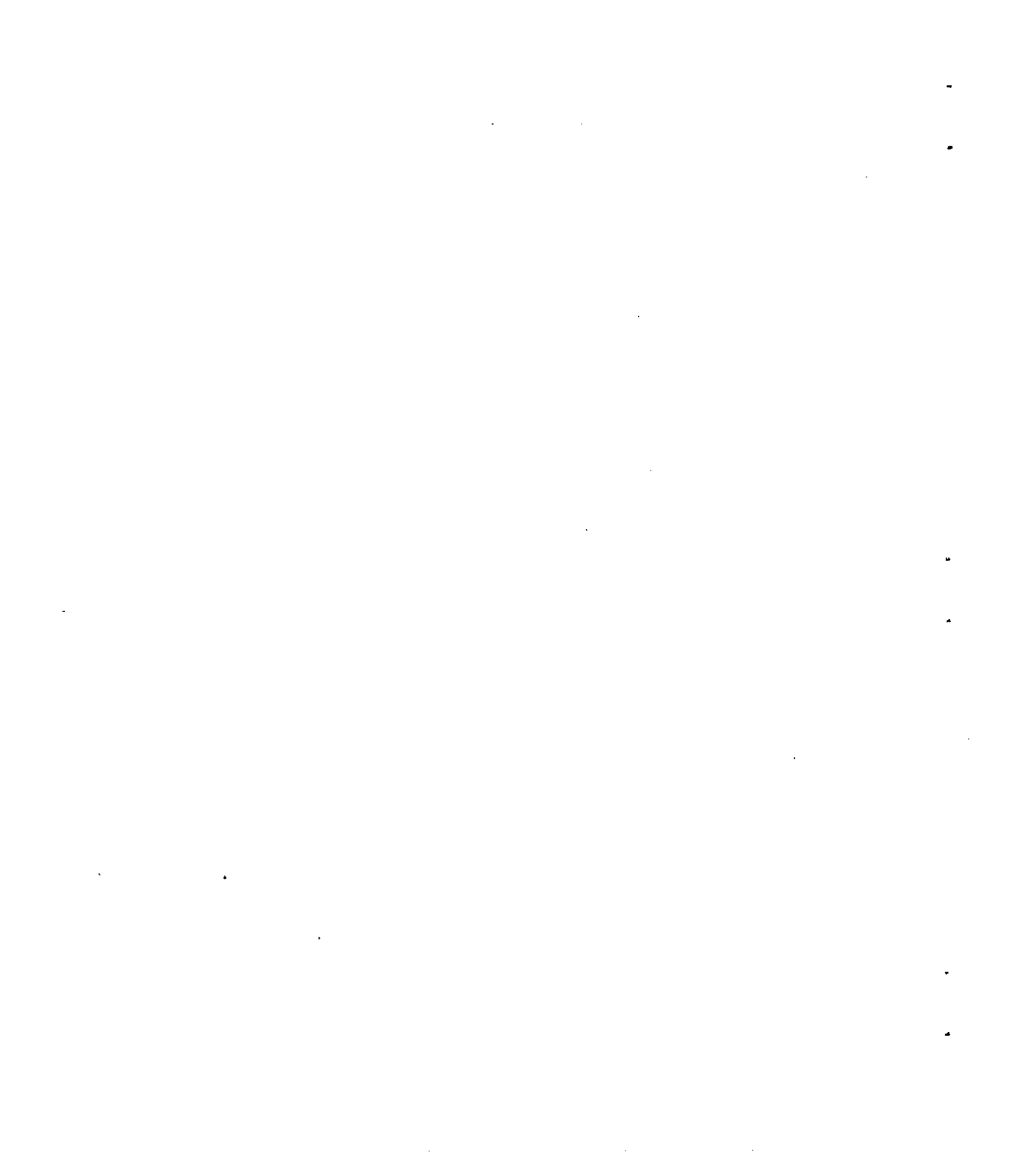
(a) $\Lambda = 0^\circ, 35^\circ$.

Figure 13.- Wing-fuselage data for a series of sweptback wings having an aspect ratio 4, taper ratio 0.6, and NACA 65A006 airfoil section.



(b) $\Lambda = 45^\circ, 60^\circ$.

Figure 13.- Concluded.



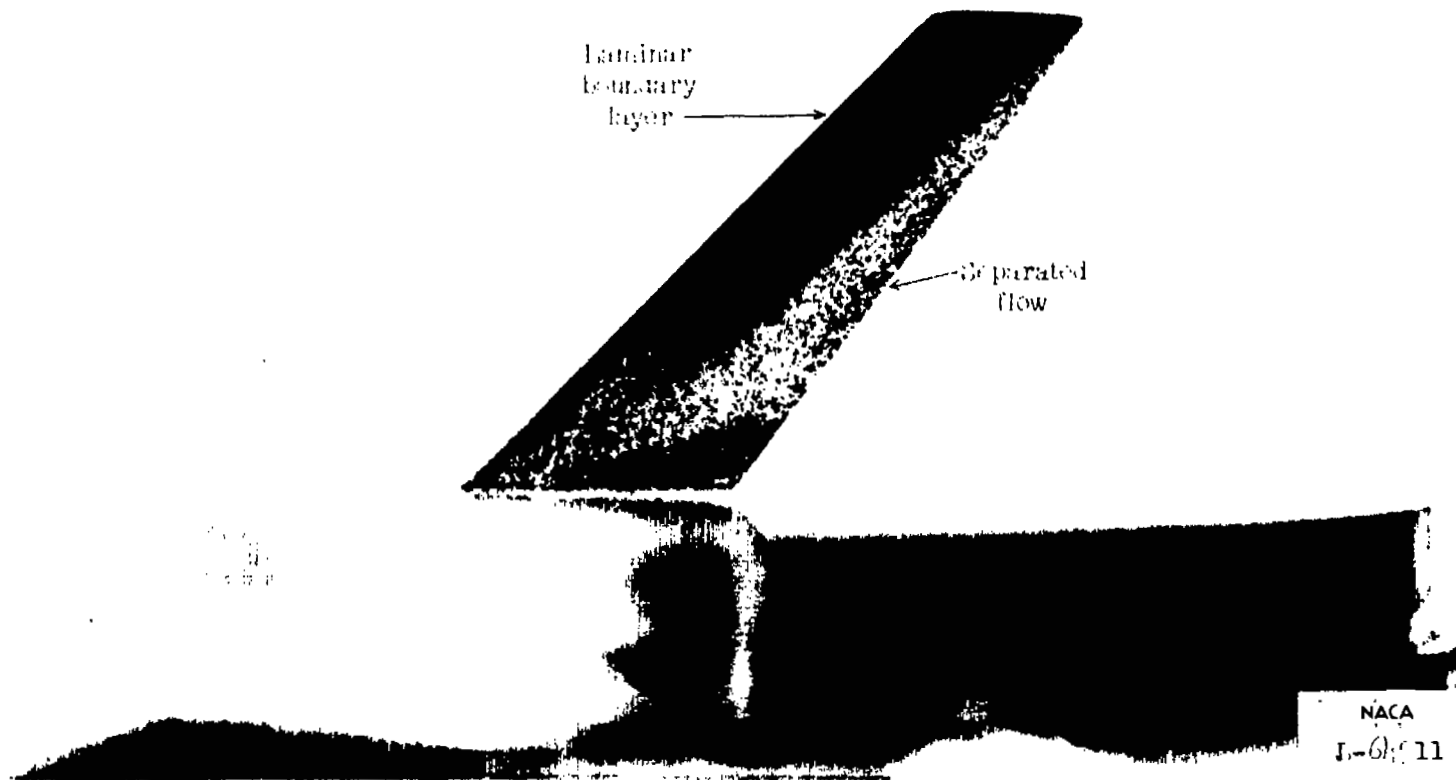
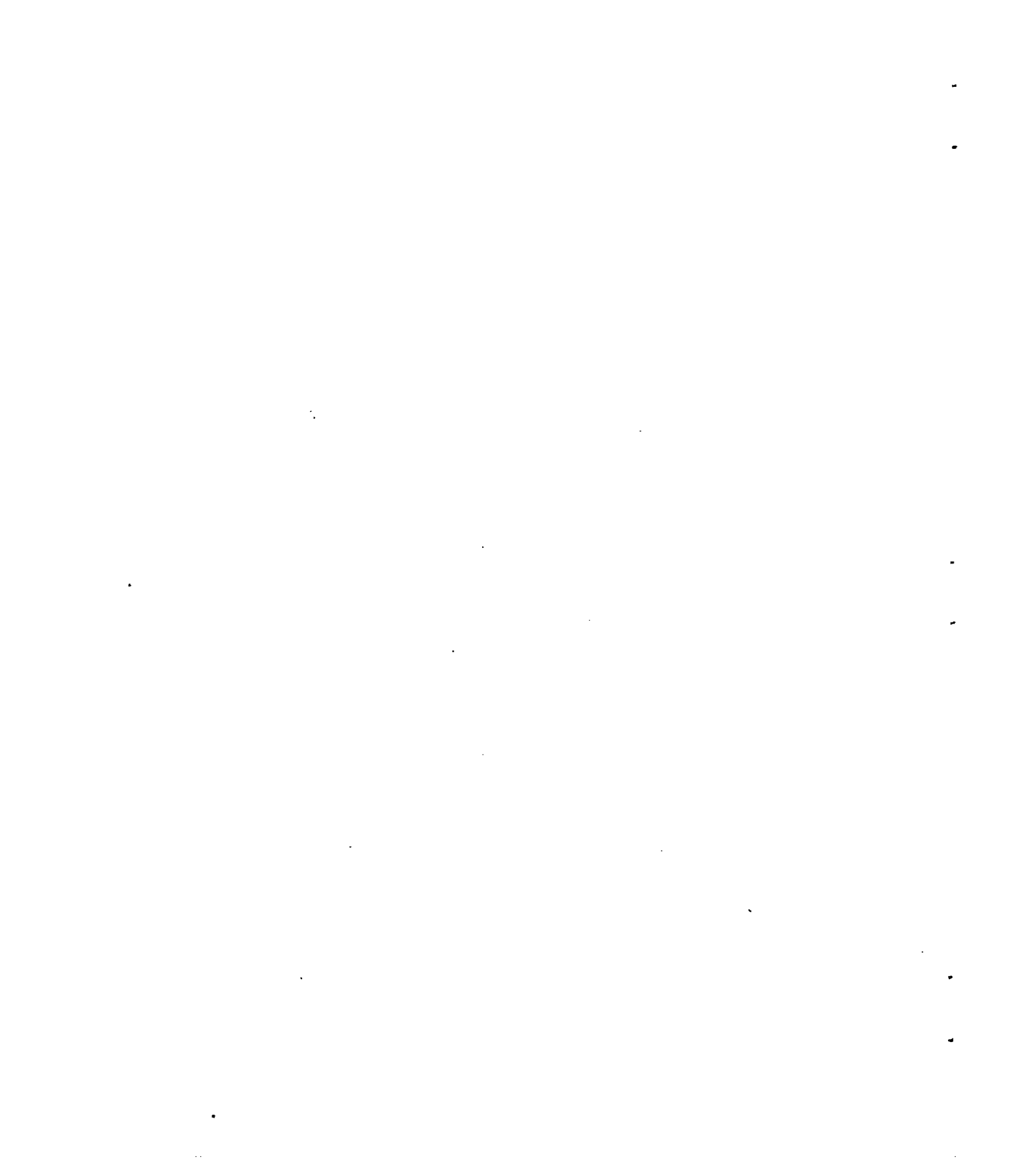


Figure 14.- A photograph showing an example of liquid film results.
 $\Lambda = 45^\circ$; $\alpha = 0^\circ$.



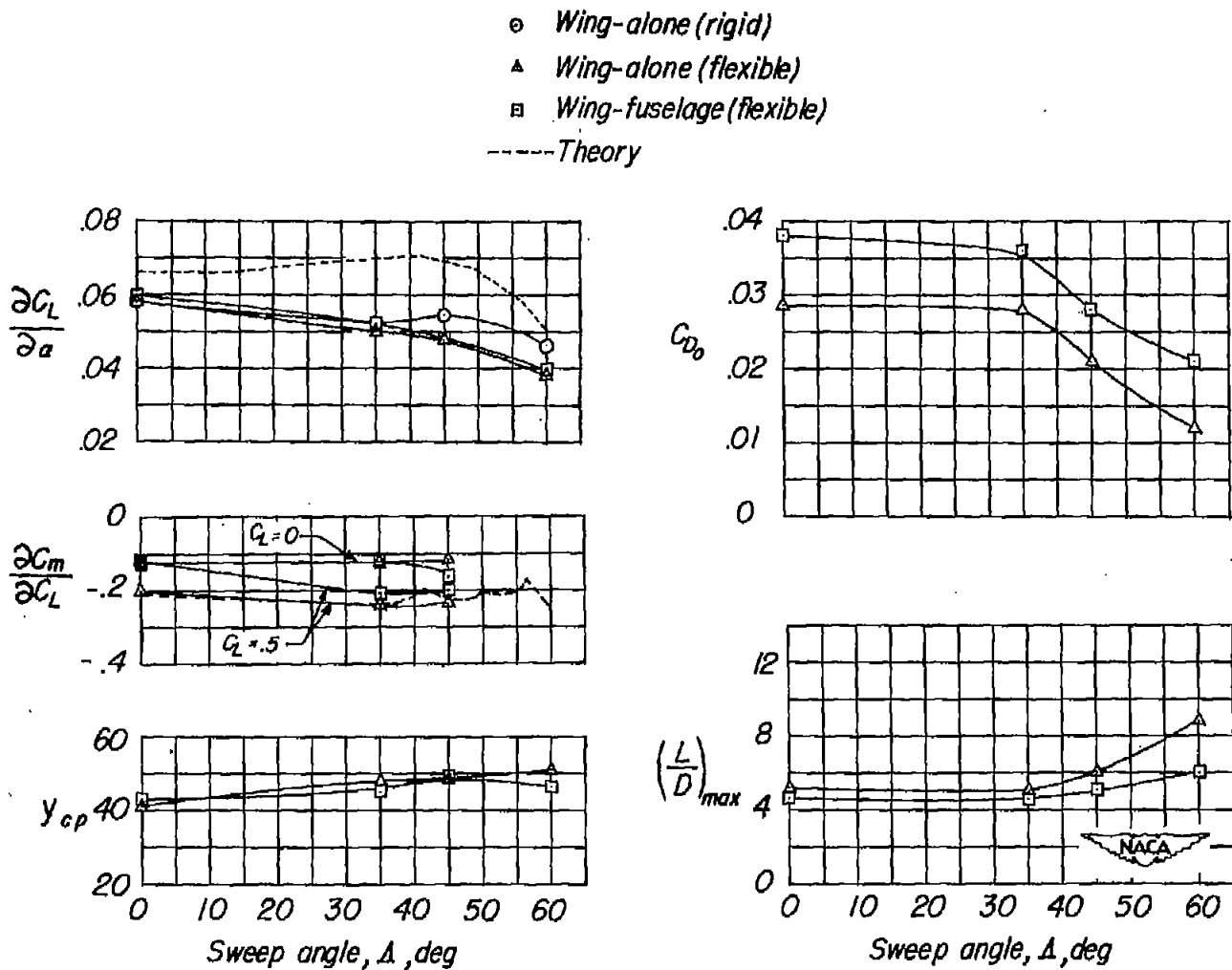


Figure 15.- Summary of the aerodynamic characteristics for a series of sweptback wings having an aspect ratio of 4, taper ratio of 0.6, and NACA 65A006 airfoil section.

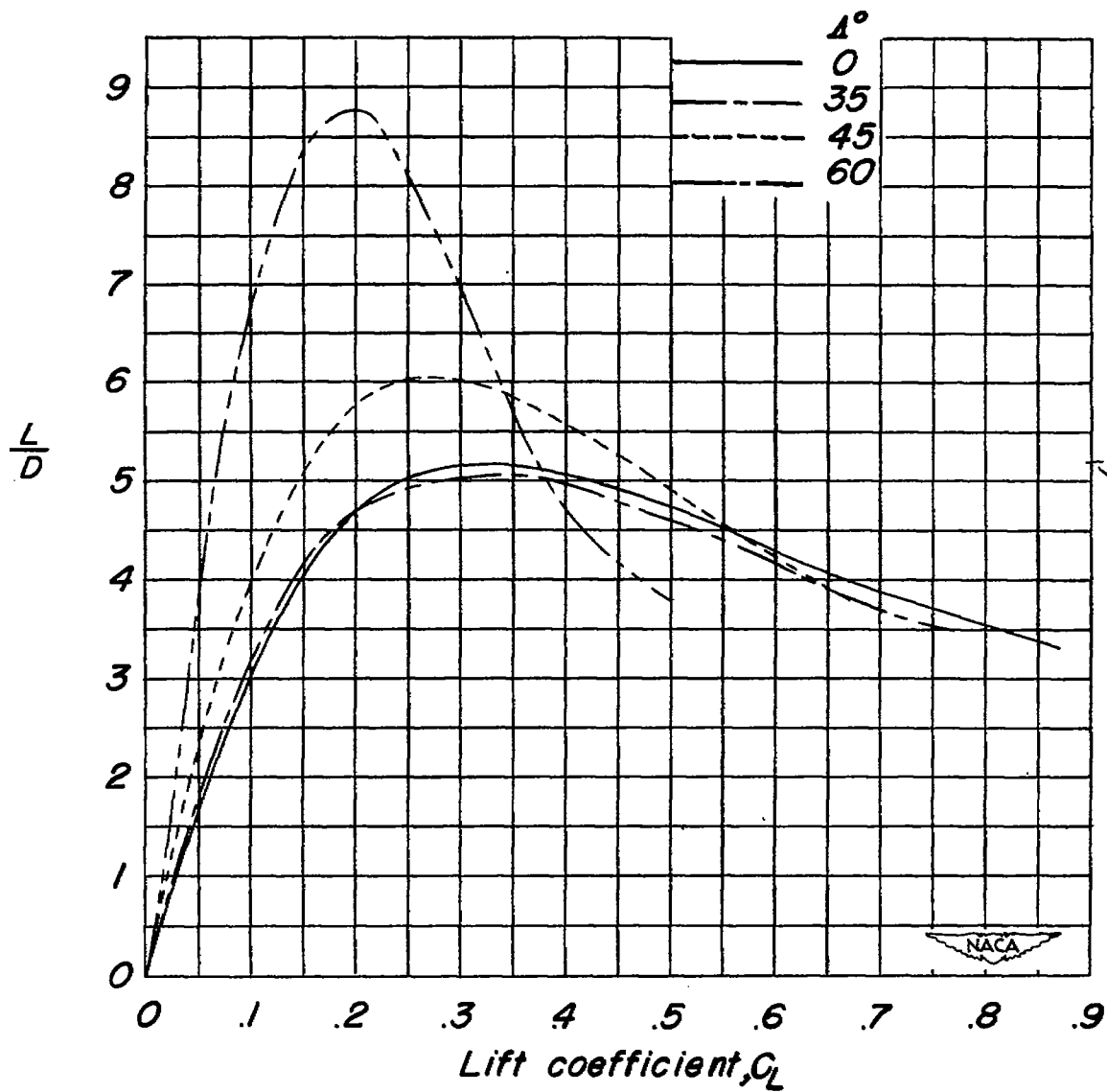


Figure 16.- Variation of lift-drag ratio with lift coefficient, wings alone.

- \triangle — Wing-alone (flexible)
 \square — Wing-fuselage (flexible)
 \odot — $\frac{1}{C_L \alpha}$ for wing-alone (rigid)
 - - - Theory

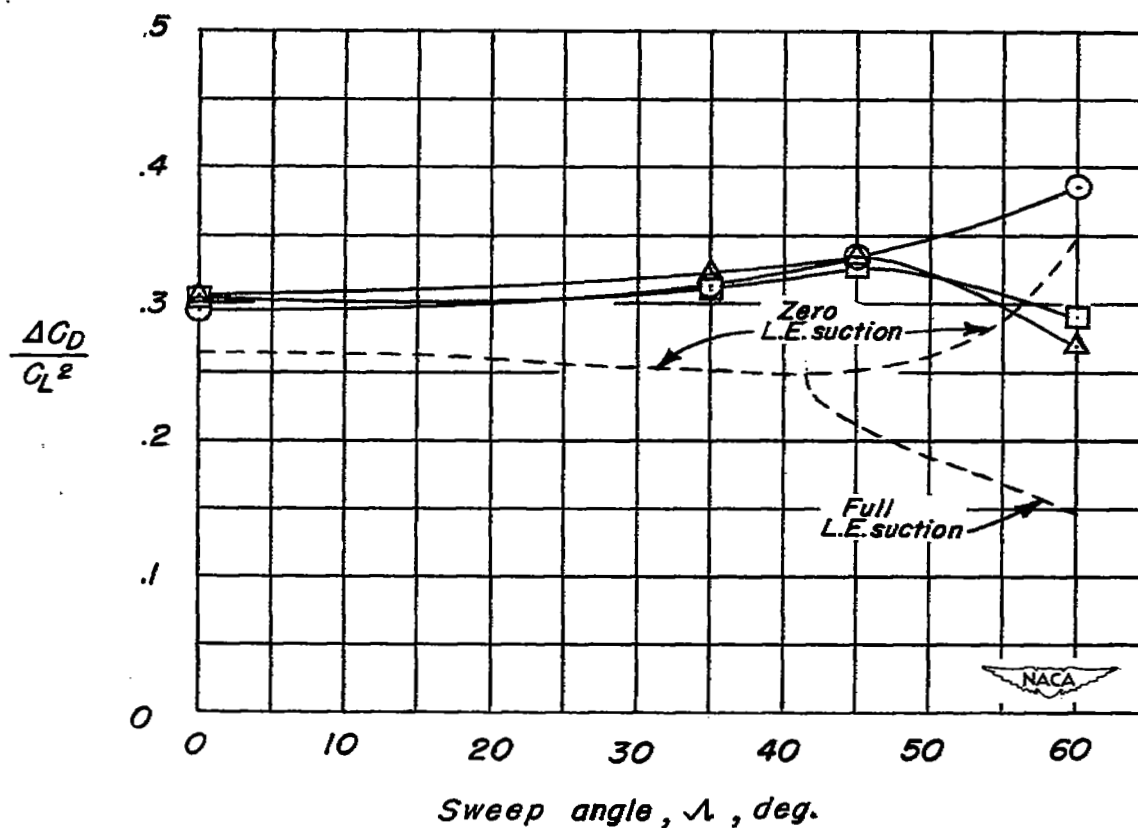


Figure 17.- Summary of drag-rise characteristics for a series of sweptback wings having an aspect ratio of 4, taper ratio of 0.6, and NACA 65A006 airfoil section.

NASA Technical Library



3 1176 01436 8030